Space Weather

RESEARCH ARTICLE
10.1029/2025SW004718

Special Collection:
Space Weather Events of 2024 May 9-15

The Impact of the 2024 Mother's Day Storm on Aircraft Surveillance Across Europe

Erik Schmölter[1] and Jens Berdermann[1]

[1]German Aerospace Center, Institute for Solar-Terrestrial Physics, Neustrelitz, Germany

Abstract The Mother's day storm from 10–13 May 2024 is one of the most extreme space weather events recorded in recent decades and triggered a strong ionospheric response with various impacts on communication and navigation systems. In this study the impact on the aviation sector, and more specifically air traffic management, is investigated with Automatic Dependent Surveillance-Broadcast (ADS-B) data from the OpenSky network. For that purpose, the event is presented with solar radiation and wind observations to describe the space weather conditions. Further, the spatial and temporal variations of the ionospheric response over Europe are analyzed with total electron content (TEC) maps and the performance of positioning via Global Navigation Satellite Systems (GNSS) is examined with 100 reference stations. These analyses show well-known space weather impacts including TEC perturbations, sudden ionospheric disturbances, signal-loss and degraded GNSS performance. Consequently, these effects are also expected for the GNSS positions transmitted via ADS-B, and the analysis confirms that a higher frequency of such anomalies occurs along flight tracks during the event (increase of up to 2.55%). These anomalies may manifest as data gaps or as position errors of various types, which in turn could decrease the visibility and awareness of participants in shared air spaces. The correlation between space weather and anomalies in ADS-B, as also shown in preceding studies, is thus further substantiated and motivates for follow-up research that combines application-specific data like ADS-B with commonly used ionospheric observations.

Plain Language Summary In May 2024, a strong space weather event affected communication and navigation systems across Europe. This study investigates how this storm impacted the aviation industry, specifically air traffic management, by looking at data from planes and Global Navigation Satellite Systems to understand the storm impact. The results show that the storm caused problems with positioning, leading to temporary gaps in data or errors. This in turn can make it harder for pilots to navigate safely and efficient. Overall, the research highlights the importance of monitoring space weather and its potential impact on critical infrastructure like air traffic control systems.

Key Points:

- Well-known space weather impacts are observed for GNSS reference station in Europe during the 2024 Mother's day storm
- Aircraft surveillance is impacted by space weather-driven anomalies during the 2024 Mother's day storm
- ADS-B data can contribute to new space weather products, well suited to predict temporal and regional impacts in aviation

Correspondence to:
E. Schmölter,
Erik.Schmoelter@dlr.de

Citation:
Schmölter, E., & Berdermann, J. (2025). The impact of the 2024 mother's day storm on aircraft surveillance across Europe. *Space Weather*, *23*, e2025SW004718. https://doi.org/10.1029/2025SW004718

Received 12 SEP 2025
Accepted 10 NOV 2025

Author Contributions:
Conceptualization: Erik Schmölter, Jens Berdermann
Formal analysis: Erik Schmölter, Jens Berdermann
Funding acquisition: Jens Berdermann
Methodology: Erik Schmölter
Project administration: Erik Schmölter, Jens Berdermann
Software: Erik Schmölter
Validation: Erik Schmölter
Visualization: Erik Schmölter
Writing – original draft: Erik Schmölter, Jens Berdermann
Writing – review & editing: Erik Schmölter, Jens Berdermann

1. Introduction

The Mother's day storm from 10 to 13 May 2024 during solar cycle 25 represents one of the most extreme space weather events recorded in recent decades (last space weather events of comparable severity occurred during the superstorms on 13 March 1989 and 30 October 2003). The several days lasting geomagnetic storm was driven by two interplanetary coronal mass ejections (CME), which interacted strongly with Earth's upper atmosphere causing a significant ionospheric response (Lee et al., 2025; Pal et al., 2025; Paul, Haralambous, et al., 2025; Paul, Moses, et al., 2025). Additionally, several *M*-class and four *X*-class flares with variations across the whole solar spectrum occurred (Kruparova et al., 2024), which further disturbed the ionosphere (Ang et al., 2025). These processes impacted our technological infrastructure with well-known disruptions to communication and navigation systems (Ishii et al., 2024). For example, the operational range of high frequency (HF) radio communication was disrupted or significantly narrowed for some regions (Gonzalez-Esparza et al., 2024) and the performance of Global Navigation Satellite Systems (GNSS) was globally degraded (Bezerra et al., 2025; Danilchuk et al., 2025). Since these are key technologies for all transportation systems, an impact in aviation, among other applications, is also expected (Xue et al., 2024).

Space weather can impact aviation by disrupting communication, navigation, and surveillance systems, as well as posing radiation hazards (Xue, 2025). This study focuses on Automatic Dependent Surveillance (ADS), a method that relies on aircraft positions determined by GNSS receivers on board aircraft. The operational impacts of space weather on aviation, or more specifically air traffic management, can include flight rerouting and cancellations,

increased flight times due to reliance on backup navigation aids, reduced airspace capacity as well as increased workload for air traffic controllers (Xue et al., 2023). These in turn can cause increased economic costs and may pose a risk to flight safety. Therefore, a comprehensive understanding of space weather impacts on air traffic management is crucial and should be grounded in the data routinely utilized by pilots and air traffic controllers. For this reason, data from the ADS system, which continuously tracks the GNSS positions and other parameters of participants in the airspace, are of particular interest. These data can reveal anomalies in flight tracks (Tabassum et al., 2017), which can be caused most notably by human-caused interference (McCallie et al., 2011; Pleninger et al., 2025; Riahi Manesh & Kaabouch, 2017) and space weather (Schmölter & Berdermann, 2024b; Schmölter et al., 2025).

Schmölter et al. (2025) investigated anomalies in ADS-B (Broadcast) during a solar flare event, analyzing selected flight tracks and demonstrating that data gaps and position errors coincided with the flare's impact. Both ADS-B and GNSS signals can be disrupted (particularly during the peak of a solar flare) leading to interruptions in aircraft tracking and resulting in significant data gaps. Additionally, sudden ionospheric disturbances, reflected in gradients and rates of total electron content (TEC), were found to coincide with position offsets, jumps, and deviations along the analyzed flight tracks. These findings indicate how degraded GNSS performance due to space weather can affect ADS systems.

The present study extends this investigation to the geomagnetic storm, whose strong ionospheric disturbances could also cause anomalies in ADS-B. Furthermore, a *X*-class solar flare during the Mother's day storm is also analyzed in detail, since short-term disturbances are more easily distinguished from non-space weather driven effects. For that purpose, observations of the solar spectrum, solar wind, ionosphere and GNSS reference station performance are applied to present the impact throughout the European region, which allows a detailed comparison with the anomalies along ADS-B flight tracks. The main aim of the present study in this regard is to quantify the event's impact on ADS-B and to describe the spatial and temporal extent. In other words, to expand the analysis from individual flight tracks to an investigation of the entire region.

The first part of the paper presents the Mother's Day storm through various space weather data sets to identify periods for detailed analysis. The second part presents the effects of the geomagnetic storm and solar flares on TEC and the performance of GNSS reference stations, providing insights into impacts likely experienced by users (e.g., via GNSS receiver on board aircraft). The next section explores anomalies in ADS-B data by showing examples of affected flight tracks and introducing methods to quantify occurrences of data gaps and position errors. All findings are discussed with an emphasis on implications for future analyses and possible contributions to space weather services.

2. Data

This study applies satellite- and ground-based measurements to describe the space weather conditions during the Mother's day storm. The impact on aircraft tracking is investigated with ADS-B tracks.

2.1. Solar Spectrum

This study uses measurements of the solar extreme ultraviolet (EUV) and X-ray radiation by the Geostationary Operational Environmental Satellites of the *R* Series (GOES-R) to describe the solar activity and magnitude of solar flares during the Mother's day storm. The EUV and X-ray Sensors (EXIS) on board these satellites (Machol et al., 2020) include the GOES X-Ray Sensor (XRS), which measures two bandpass channels from 0.05 to 0.4 nm and from 0.1 to 0.8 nm (Chamberlin et al., 2009), and the GOES EUV Sensor (EUVS), which measures seven solar emission lines and the Mg II core-to-wing ratio (Eparvier et al., 2009). The XRS observations are used to classify solar flares according to the National Oceanic and Atmospheric Administration (NOAA) Space Weather Prediction Center (SWPC) scale and were applied by various studies to describe the solar activity during the event (Kruparova et al., 2024; Paul, Moses, et al., 2025). The GOES-R EXIS data are available via the NOAA National Geophysical Data Center (NGDC) web interface (NGDC, 2025).

This study further uses solar radio flux measurements (SFX) by the solar flux telescope at the Geodetic Observatory Wettzell (GOW) in southern Germany (49.14°N, 12.87°E). This telescope, which is operated by the Federal Agency for Cartography and Geodesy (BKG), measures six frequencies from 1.4 to 4.9 GHz including the commonly used solar radio flux index F10.7 (Tapping, 2013) at the frequency of 2.8 GHz. Additionally, the lower

frequencies are close to the GNSS bands, which allows to identify solar radio burst, that could interfere GNSS signals and cause degraded positioning performance. This was successfully shown for a different event by a preceding study about space weather impacts on aviation (Schmölter et al., 2025). Another measurement campaign successfully investigated the integrity of GNSS using data from the telescope (Binder et al., 2025). For that reason, the SFX data provide sufficient insights for the purpose of this study. More in-depth analysis of the solar radio burst during the Mother's day storm are provided by other studies (Kruparova et al., 2024), which include measurements of various satellite missions. The SFX data are available via the BKG web page (BKG, 2025).

2.2. Solar Wind and Interplanetary Magnetic Field

This study uses solar wind and interplanetary magnetic field (IMF) measurements to characterize the resulting geomagnetic activity during the Mother's day storm, with a particular focus on storm sudden commencements (associated with the most significant space weather impacts). For this purpose, the times from the near-Earth interplanetary CME list (Cane & Richardson, 2003; I. G. Richardson & Cane, 2010; I. Richardson & Cane, 2024) are presented along data from National Aeronautics and Space Administration's (NASA) Advanced Composition Explorer (ACE) satellite mission (Stone et al., 1998; Zwickl et al., 1998). The Solar Wind Electron, Proton, and Alpha Monitor (SWEPAM) on board this satellite measures the solar wind plasma electron and ion fluxes (McComas et al., 1998) and the Magnetic Field Experiment (MAG) measures the six magnetic field vectors of the IMF. The ACE data are provided through the NASA ACE Science Center (Garrard et al., 1998) web page (ASC, 2025).

The resulting geomagnetic activity is presented with the planetary *Kp* index. This index measures the disturbances of the horizontal component of Earth's magnetic field (Matzka et al., 2021) and is applied for the NOAA space weather scale to classify geomagnetic storms. *Kp* index data are provided the German Research Center for Geosciences (GFZ) Potsdam (GFZ, 2025) and are part of the NASA Goddard Space Flight Center's (GSFC) OMNI database, that can be accessed through the OMNIWeb interface (NASA, 2025). Geomagnetic activity levels are classified following the criteria of Loewe and Prölss (1997).

In this study, a general understanding of the geomagnetic storm is sufficient, as the focus is primarily on the timing and its impact on ionospheric parameters. More detailed analyses of geomagnetic activity during the event are reported by De Michelis and Consolini (2025).

2.3. GNSS Observations

Global, near real-time TEC Maps are provided by the Ionosphere Monitoring and Prediction Center (IMPC), which describe the integrated plasma density of the ionosphere as a regular grid of 2.5° × 5.0° (Jakowski et al., 2011; Jakowski & Jungstand, 1994; Kriegel & Berdermann, 2020). The generation of the TEC maps includes several data products, that are applied in this study. (a) Ground-based GNSS measurements are collected from networks of geodetic receivers (e.g., the International GNSS Service) and are well-suited to describe the impact of the Mother's day storm on the GNSS positioning performance. (b) Vertical TEC is calculated at ionospheric piercing points (IPP) along available satellite-receiver links based on the ground-based GNSS measurements. These observations cover the European region sufficiently and are applied in this study to describe the rapid ionospheric response to solar flares. (c) The vertical TEC is assimilated into Neustrelitz Total Electron Content Model (NTCM) resulting in the final TEC map, which can be used to calculate further ionospheric parameters including gradients. These are of particular interest to investigate the space weather impacts along flight tracks (Schmölter & Berdermann, 2024b; Schmölter et al., 2025). The near real-time TEC Map, the NTCM TEC map and the calibrated VTEC measurements are available via the IMPC web page (IMPC, 2025).

2.4. Aircraft Tracks

The International Civil Aviation Organization (ICAO) introduced ADS-B as a new approach to monitor the global airspace (ICAO, 2014; ICAO, 2016) and to ensure safe and efficient air traffic management. For that purpose, each aircraft broadcasts its GNSS position and additional information (e.g., flight number, aircraft type and speed) in short time intervals via messages. These messages are transmitted at a frequency of 1,090 MHz (agreed international link) and can be received by ground stations or other aircraft. This provides nearby participants in the airspace with a better situational awareness and visibility. Furthermore, it enables tracking of

aircraft en route and storing these tracks in databases. Access to historical ADS-B data, which enable various research (Schäfer et al., 2021), is provided by OpenSky, which is a participatory network of ADS-B receivers deployed at homes and organizations of volunteers (Schäfer et al., 2014). The received ADS-B messages through this network are collected in a historical database, whose data access is introduced at the OpenSky web page (OpenSky, 2025).

During the period examined in this study, from 10–13 May 2024, more than 18,000 different aircraft were tracked in Europe, and a total of around 700 million ADS-B messages were recorded. Such amounts of application-related data are rarely available for space weather studies.

2.5. Data Processing

The space weather data analyzed in this study do not require any additional processing and are presented to complement and confirm previous studies on the Mother's day storm (Ang et al., 2025; Pal et al., 2025; Paul, Haralambous, et al., 2025; Paul, Moses, et al., 2025; R. Singh et al., 2024; Suraina et al., 2025; Wang et al., 2025). In contrast, the ADS-B data are processed in a specific way to allow the analysis of space weather impacts. For this analysis, ADS-B data downloaded from the OpenSky historical database are stored in 1-min files, each containing all available data fields (e.g., timestamp, ICAO aircraft identifier, latitude, longitude, velocity, and heading). These data can be filtered (e.g., for the European region) and summarized to global parameters like aircraft or ADS-B message count per minute via the number of unique ICAO identifiers or entries in each file, respectively.

The trajectory parameter for various flight tracks are recorded across several 1-min files. Therefore, an analysis of individual flight tracks requires merging the entries corresponding to each aircraft's unique ICAO identifier to form continuous trajectory time series. These time series can be analyzed for parameters like the distance traveled and changes in heading between reported positions, but also for anomalies such as position errors and data gaps. The specific approach for each parameter is explained in the respective parts in Section 3.3.

3. Results

The results are presented in three sections, which provide a general overview of the solar activity during the Mother's day storm, describe the ionospheric response, and then examine the ADS-B tracks in detail.

3.1. Solar Activity During the Mother's Day Storm

On 10–12 May 2024, a series of significant solar flares were observed, featuring four *X*-class and several *M*-class flares. Figure 1 shows the variability of the solar spectrum including X-ray, EUV and radio fluxes during the Mother's day storm. Three of the *X*-class events were observable from Europe (see Figure 1c) and occurred in combination with strong increases in the EUV spectrum, reaching levels of up to 280%, 290%, and 150%. Additional periods of notable EUV activity occurred during *M*-class flares, including the event on 12 May 2024 at 00:41 UT. The radio flux measurements in Figure 1c show also strong increases during the flares for various frequencies including 1.4 GHz close to the frequency bands used by GNSS. Thus, impacts including direct interference for GNSS receivers, positioning errors due to TEC enhancements and HF disruptions can be expected (Chen et al., 2005; Yasyukevich et al., 2018) and are reported by various studies of the event (Bezerra et al., 2025; Kruparova et al., 2024; Park et al., 2025; Paul, Haralambous, et al., 2025; Younas et al., 2025). The degraded GNSS performance may impact transportation systems (Xue et al., 2024) including aviation and in particular aircraft surveillance (Schmölter et al., 2025). Therefore, the Mother's day storm provides an excellent opportunity to analyze space weather impacts on those systems based on increases in the solar spectrum and solar wind conditions.

In Figure 2a the solar wind plasma density n_p (black) and speed v_p (blue) with maxima of approximately 60 cm^{-3} and 1,000 $km{\cdot}s^{-1}$ during the Mother's day storm are shown. The magnitude B_m (black) and z component B_z (red) of the IMF are shown in Figure 2b highlighting the strong southward direction during the event allowing efficient coupling of the solar wind into Earth's magnetic field. This in turn caused one of the strongest geomagnetic storms recorded (Paul, Moses, et al., 2025) with severe and extreme conditions (*Kp* greater 7) for approximately 33 hr during 10–11 May 2024 (see Figure 2c). The storm sudden commencements according to the Richardson-Cane CME list (Cane & Richardson, 2003; I. G. Richardson & Cane, 2010; I. Richardson & Cane, 2024) is indicated

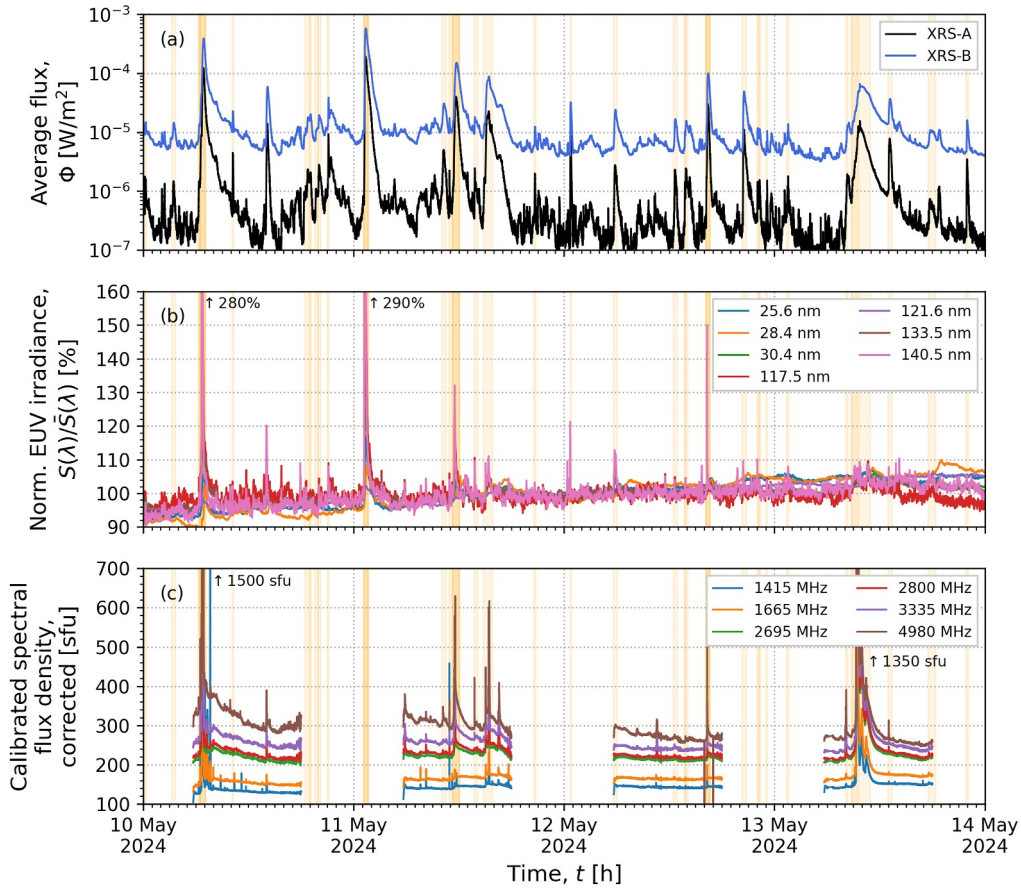

Figure 1. Solar X-ray fluxes (a) and normalized EUV irradiances (b) measured by GOES as well as radio fluxes measured by Geodetic Observatory Wettzell (c) during the Mother's day storm 2024. EUV irradiances are normalized as means vary substantially across different wavelengths. Solar flares of the classes *X* and *M* are shaded orange.

with the darker blue shading in Figure 2. During the storm, strong ionospheric gradients are expected, which affect the positioning accuracy of GNSS. Schmölter et al. (2025) presented such impacts for the aircraft tracking using selected examples. Further, Schmölter and Berdermann (2024b) investigated the increased number of lateral deviation events occurring in aircraft surveillance due to degraded tracking caused by such gradients. The Mother's day storm offers an excellent opportunity for more detailed investigations of space weather driven disturbances.

3.2. Ionospheric Response During the Mother's Day Storm

The ionospheric response to the Mother's day storm is described by various studies for the global (Pal et al., 2025; Paul, Haralambous, et al., 2025; Paul, Moses, et al., 2025) and regional ionosphere (Ang et al., 2025; R. Singh et al., 2024; Suraina et al., 2025; Wang et al., 2025). Nonetheless, the effects for the European region are briefly discussed in this study using IMPC TEC maps. This allows to identify the impacted sub regions of the geomagnetic storm starting 10 May 2024 17:05 UT and *X*-class solar flare on 11 May 2024 from 11:15 to 12:05 UT. A brief discussion of the observed degradation of PPP performance is also presented, since GNSS receivers on board of aircraft are similarly affected as the reference stations.

Figure 3 shows the TEC response between 10°W and 30°E for latitudes from 30° to 80°N. The diurnal variation is dominant in Figure 3a, but small-scale features also occur (especially during the initial storm sudden commencement). TEC values at noon on 11 May 2024 are significantly lower compared to the previous and next day. The negative phase of the storm dominates the ionospheric state during this period. Strong perturbations occur in high latitudes, which extend further south to mid latitudes during the main phase of the storm (see black

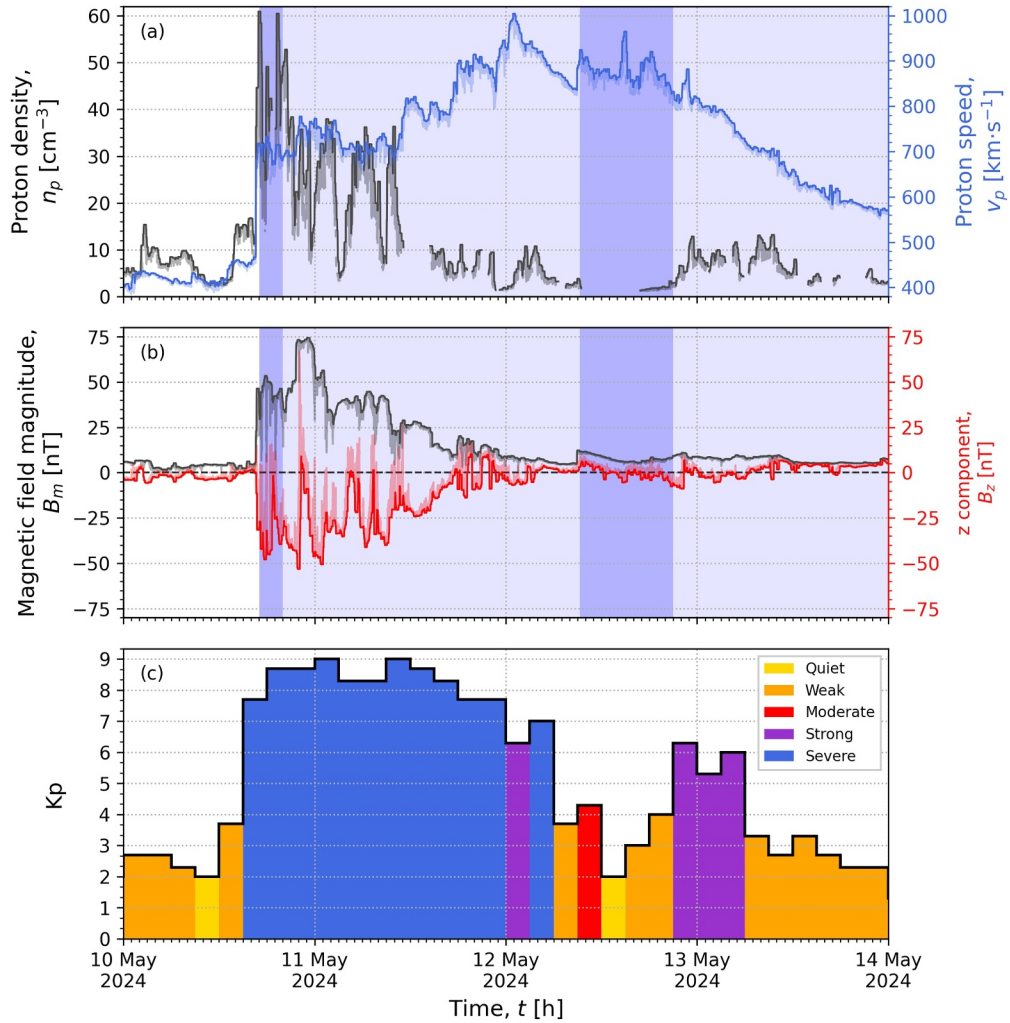

Figure 2. Solar wind (a), interplanetary magnetic field (b) and geomagnetic activity (c) during the Mother's day storm 2024. The raw data of proton density n_p (black) and speed v_p (blue) in panel (a) as well as magnetic field magnitude B_m (black) and z component B_z (red) in panel (b) are shown with the transparent time series, while hourly maxima (n_p, v_p and B_m) and minima (B_z) are shown with the opaque time series. The light blue shading indicates the storm period and the darker blue shading highlights the storm sudden commencements. The *Kp* index in panel (c) highlights the levels of geomagnetic activity.

curve between vertical lines in Figure 3b). These features are also reported by Paul, Haralambous, et al. (2025) using various ionospheric observations.

The impact of a selected *X*-class flare is presented with VTEC measurements. Figure 4a shows the radio flux at the frequency of 1.4 GHz compared to the number of ionospheric piercing points (IPP), which reflects the number of satellite-receiver links. An extended and strong decrease of these links occurs approximately at 11:45 UT in correlation with enhancements in the radio flux (to a lesser degree also at 11:15 UT). This indicates the direct interference during the solar flare. Figure 4b shows this interruption of satellite-receiver links with the observed vertical TEC. Up to 53% of the links are lost for a time span between 1 and 5 min and restored when the radio flux returns to lower levels. The regional impact of this disruption is further presented in Figure 4c by showing the VTEC difference map (1° × 1°) for two time intervals, from 11:41:30 to 11:42:00 UT (undisturbed) and from 11:44:30 to 11:45:00 UT (disturbed). A significant decrease is observed south of 50°N and centered at approximately 5°E (coincides with locations at 12:00 LT). Thus, the flare impact occurs southward of the ionospheric disturbances resulting from the geomagnetic storm (see Figure 3b). The signal interruption has an impact on VTEC with deviations of up to 40 TECU in these regions (see Figure 4d). It is important to note, that

10.1029/2025SW004718

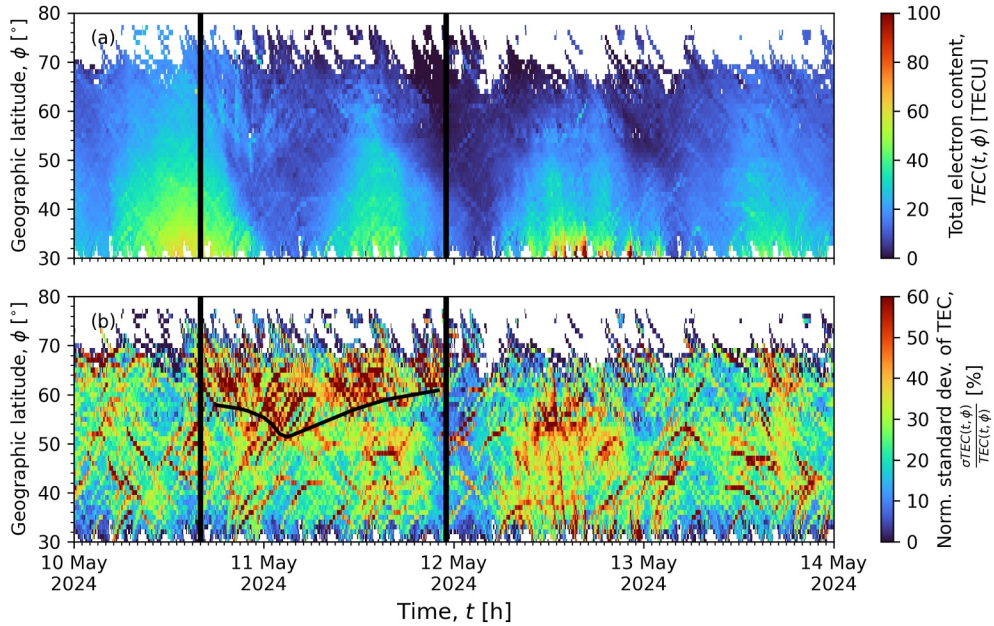

Figure 3. The mean total electron content TEC (a) and the normalized standard deviation σTEC/TEC (b) calculated between 10°W and 30°E. The vertical lines mark out the period of severe geomagnetic activity. The curve between these two lines indicates the furthest extent of TEC perturbations from high to mid latitudes.

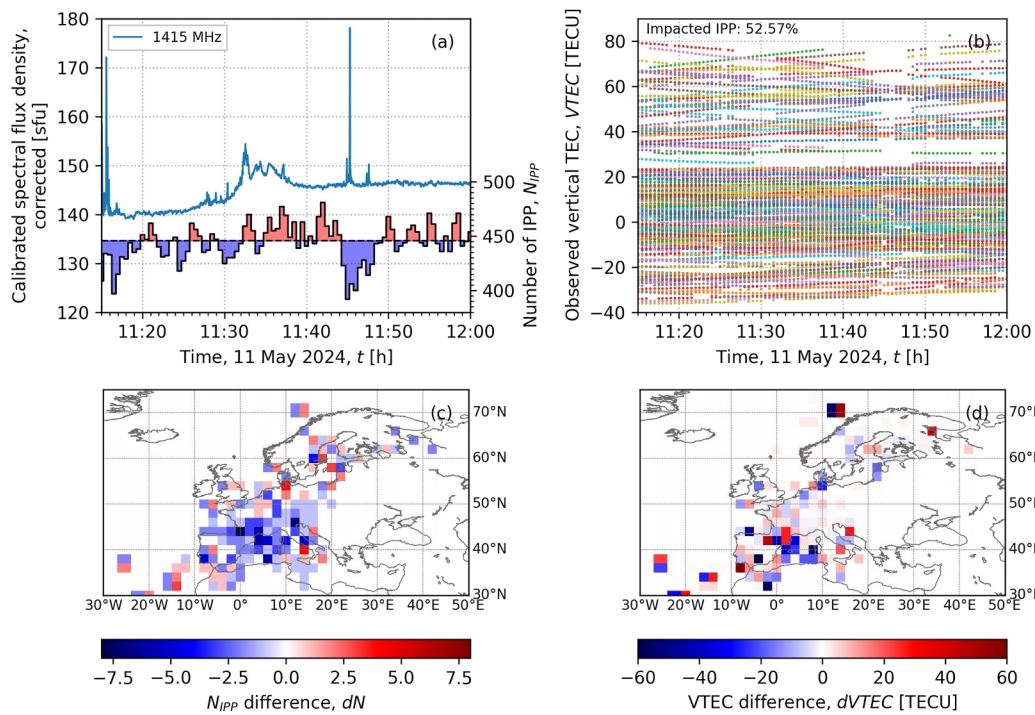

Figure 4. Radio flux and number of ionospheric piercing points n_{IPP} (a), observed vertical TEC VTEC (b), n_{IPP} difference map (c) and VTEC difference map (d). The red and blue color coding in panel (a) indicates values greater and smaller than the mean, respectively.

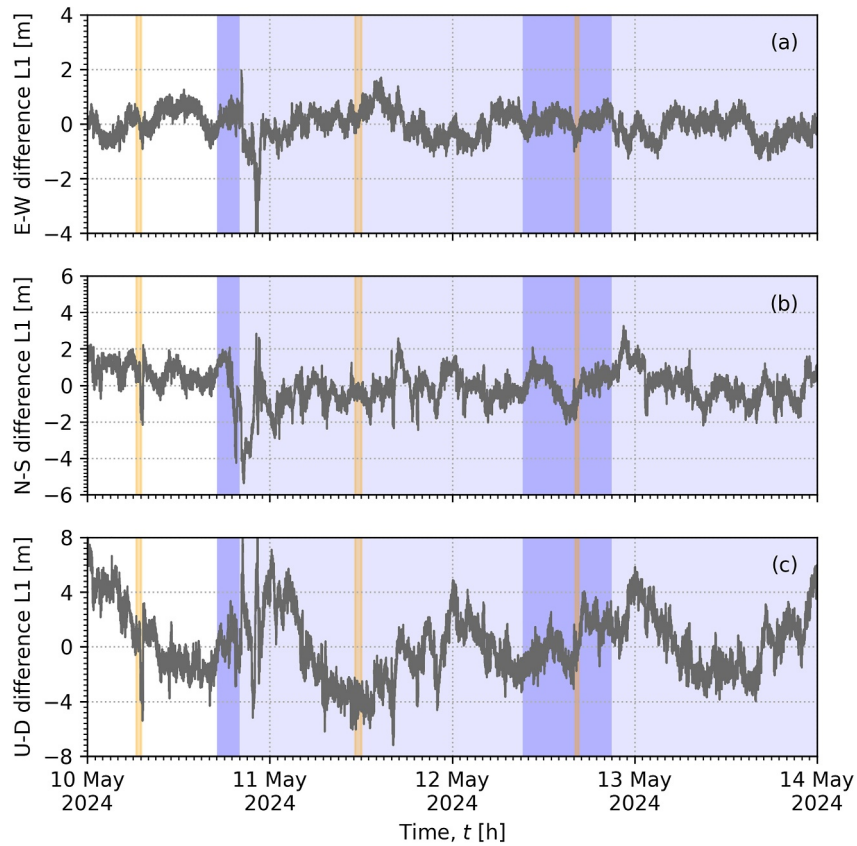

Figure 5. The single-frequency position errors in East-West (a), North-South (b) and Up-Down (c) directions are shown for the reference station Rostock-Warnemünde in Germany (WARN00DEU) during the Mother's day storm 2024. Solar flares of the classes *X* are shaded orange. The light blue shading indicates the storm period and the darker blue shading highlights the storm sudden commencements.

interference-driven variations must be distinguished from ionization-driven TEC changes during the flare, which typically persist for several minutes after the peak (Berdermann et al., 2018).

The impact of the geomagnetic storm and solar flares is further analyzed using the position errors of a reference station. For this purpose, single-frequency positioning is performed using Global Positioning System (GPS) data along with corrections from the broadcast ephemeris. Figure 5 shows position errors in North-South, East-West and Up-Down directions for the station Rostock-Warnemünde in Germany (WARN00DEU). A clear variation over several meters in all directions occurs after the initial storm sudden commencement. The impact of the TEC perturbations from high to mid latitudes (see Figure 3) is therefore confirmed for this station. The *X*-class solar flare on 11 May 2024 shows no significant deviations, which is in good agreement with the observed flare impact region (see Figure 4c). The solar flare on 10 May 2024 with even stronger radio flux (see Figure 1c) shows a deviation over several meters though, especially in the North-South and Up-Down directions. Further, the general positioning performance is estimated with the root mean square errors (RMSE), which are combined to a total value according to

$$RMSE_{Pos} = \sqrt{RMSE_{E\text{-}W}^2 + RMSE_{N\text{-}S}^2 + RMSE_{U\text{-}D}^2}\,[\mathrm{m}]. \quad (1)$$

For the station in Rostock-Warnemünde daily $RMSE_{Pos}$ of 3.02, 2.88, 1.94, and 2.35 m are estimated during 10–13 May 2024. Although these disturbances are relatively minor compared to other reference stations, the variations caused by the Mother's day storm are distinct and exceed other impacts.

The analysis is extended by calculating $RMSE_{Pos}$ for 100 reference stations across Europe during 11 May 2024. Figure 6a shows the results, which include notable features that are further highlighted with the interpolated map

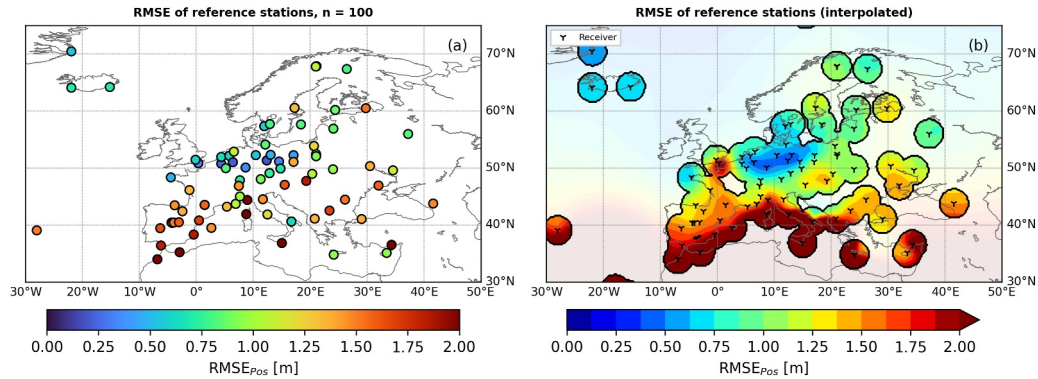

Figure 6. The root mean square errors of the single-frequency positioning $RMSE_{Pos}$ for various reference stations across Europe during the entire day of 11 May 2024 (a). The interpolated map (radial basis function interpolation with linear kernel) highlights spatial variations (b). Regions of the interpolated map, that are further away than 2.5° from the next reference station and cannot be reliably interpreted, are masked.

in Figure 6b. The lowest RMSE are observed between 50° and 60°N except for stations in the Southern United Kingdom of Great Britain. Slightly increased RMSE (approximately 1 m) are observed northward of 60°N. Southward of 50°N strong increases of the RMSE are observed dependent on longitude and values of up to 28 m occur (Noto Radio Observatory in Italy). These strong spatial differences relate to the various space weather processes, which are amplified during the Mother's day storm (see Figures 3 and 4).

Since most aircraft are still equipped with single frequency receivers, similar disturbances are expected. Data gaps during solar flares may occur for tracks due to direct interference of the GNSS or ADS-B signals (Schmölter et al., 2025; Xue et al., 2024) or degraded GNSS performance may occur due to ionospheric gradients during the geomagnetic storm.

3.3. ADS-B Tracking During the Mother's Day Storm

The impact of space weather on ADS-B tracking is analyzed through various metrics, each highlighting specific interactions between the event and key components of the system. Table 1 summarizes these metrics categorized by the distinct impacts that can be analyzed. (a) Transmission category metrics allow the detection of data gaps, thereby supporting the analysis of signal interference in GNSS and ADS-B. This involves analyzing the amount of data entries, their associated timestamps, and corresponding ICAO identifiers. (b) In-flight category metrics allow the identification of navigation and position errors along flight tracks, which in turn can be correlated with

Table 1
Metrics for the Analysis of ADS-B Tracking During the Mother's Day Storm

Category	Metric	Variable	Unit	Insight/Impact
Transmission	Message count	n_m	min^{-1}	- Ionospheric disturbances - Signal interference - Data gaps
	Aircraft count	n_a	min^{-1}	
	Message rate	n_m/n_a	min^{-1}	
Tracking In flight	Position	ϕ, λ	°	- Ionospheric disturbances - Navigation errors - Position errors
	Geodesic distance	s	km	
	Heading	θ	°	
	"Jump" count	n_j with $ds/dt > 100$ km·h^{-1} $d\theta/dt > 170°\cdot s^{-1}$	min^{-1}	
	"Jump" rate	n_j/n_a	min^{-1}	
Tracking On ground	Position	ϕ, λ	°	- Ionospheric disturbances - Position errors
	RMSE of position	$RMSE_{Pos}$	m	

10.1029/2025SW004718

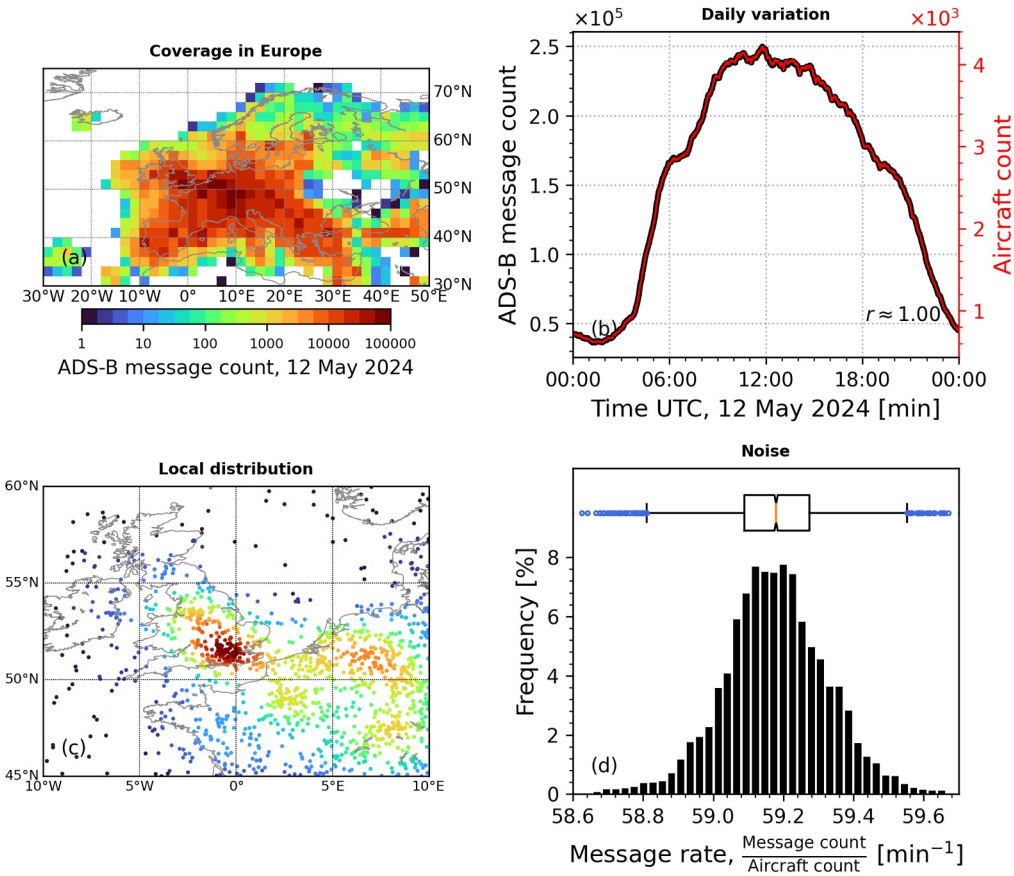

Figure 7. ADS-B message count on 12 May 2024, mapped over a 1° × 1° grid to illustrate coverage across Europe (a), corresponding daily variations (b) in the total ADS-B message count (black line) alongside aircraft count (red line), local distribution of aircraft at 12 May 2024 12:00 UT (c) and the average message rate (calculated as message count per aircraft count) using both a histogram and a box plot (d).

ionospheric disturbances. This analysis involves examining aircraft positions, traveled distances, and heading data to detect anomalies. (c) On-ground category metrics apply an approach that considers aircraft on the ground as reference stations, enabling the estimation of position errors across the European region similar to Figure 6.

The metrics are applied within the respective parts of the analysis, which also address the challenges and limitations of them for space weather impact studies. In this regard, it is also important to consider the spatial distribution and non-space weather-driven variability of the ADS-B data and to consider these in the interpretation of each metric and result.

In a global or regional analysis of ADS-B data, different variations driven by geographical and economic factors must be considered. These include, for example, distribution of ADS-B receivers, distribution and capacity of airports, day of the week, time of day, aircraft types or human-caused interference. For this reason, this study is limited to Europe, where data coverage is rather consistent for larger regions. This is highlighted with the ADS-B message count during 12 May 2024 in Figure 7a. Figure 7b shows the corresponding daily variations of the ADS-B message count and additionally the aircraft count. Both variations are strongly correlated (approximately 1.00) and occur similarly for the other days of the week. Nevertheless, the data are irregular distributed and deviate over time, which should be accounted in analyses with higher spatial or temporal resolution. Figure 7c shows the local distribution of aircraft at 12 May 2024 12:00 UT with increased densities around major airports. A proximity to airports also implies that the flight parameters change significantly (e.g., altitudes or distances flown), causing increasing complexity for statistical analyses.

Calculated rates such as message count per aircraft per minute (see Table 1) are a useful tool for identifying data gaps and were successfully applied in preceding studies (Schmölter & Berdermann, 2024b; Schmölter

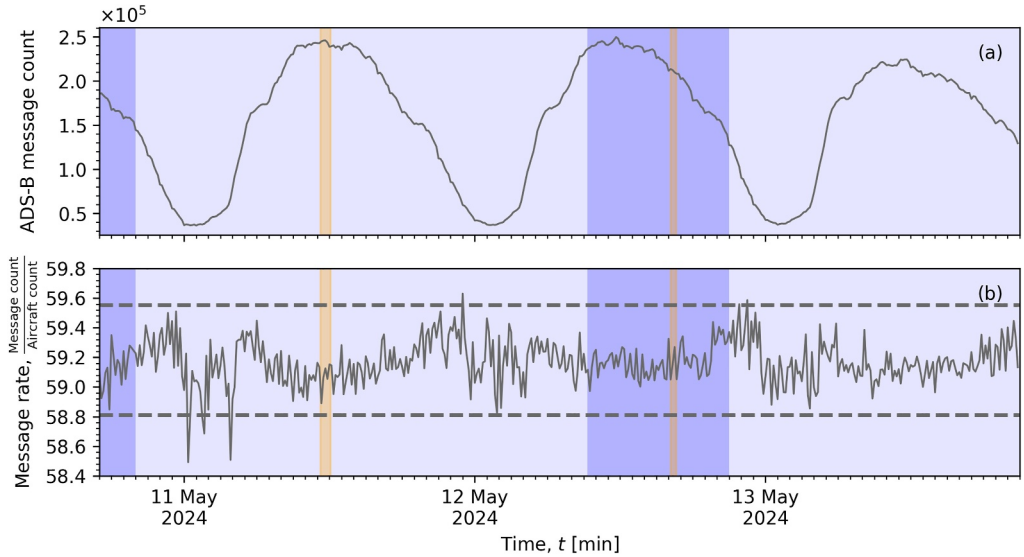

Figure 8. The total ADS-B message count (a) and rate (b) during the Mother's day storm 2024. The limits (dashed lines) up to which no outliers occur are calculated with the first quartile $Q1$, third quartile $Q3$ and inter-quartile range IQR according to $Q1 - 1.5 \cdot IQR$ and $Q3 + 1.5 \cdot IQR$. Solar flares of the classes X are shaded orange. The light blue shading indicates the storm period and the darker blue shading highlights the storm sudden commencements.

et al., 2025). However, combining such an approach with statistical analysis of an entire region must account for a varying number of flights starting, ending or being interrupted, as these introduce noise into the rate even in times without any further disturbances (e.g., space weather impacts). Figure 7d shows the noise for the European region based on the daily variations in Figure 7b.

Due to these described features of ADS-B data, this study applies averaged parameters over the entire region of Europe to identify time periods with anomalies (data gaps or position errors). The impacted flights during these anomalies are then further investigated in detail (i.e., as individual tracks) to confirm the correlation with space weather processes.

Figure 8a shows the total count of ADS-B messages following the diurnal variation (see also Figure 7b) without a notable impact of the geomagnetic storm or solar flares. However, the message rate in Figure 8b shows strong deviations and outliers according to the limits calculated with the first quartile $Q1$, third quartile $Q3$ and inter-quartile range IQR according to $Q1 - 1.5 \cdot IQR$ and $Q3 + 1.5 \cdot IQR$ (see Figure 7d). Notable outliers occur during 11 May 2024 after the storm sudden commencement (Cane & Richardson, 2003; I. G. Richardson & Cane, 2010; I. Richardson & Cane, 2024), which coincide further with the strong TEC perturbations (see Figure 3b) and degraded Precise Point Positioning (PPP) performance (see Figure 5). It should be noted that deviations of the message rate are generally greater at this time of day, as the number of aircraft is minimal (approximately 1,000). Nevertheless, there are no outliers during the other days. The minimum message rate is 1.18% smaller than the median and corresponds to an unexpected loss of approximately 3,000 messages per minute. If this loss of messages is driven by space weather impacts, then the overall impact is relatively small. However, it is important to consider that these data gaps are not evenly distributed across all flights and that significant interruptions may arise for affected aircraft (Schmölter et al., 2025).

The message rate is further investigated dependent on geographic latitude in Figure 9. The aircraft count in Figure 9a shows as expected the diurnal variation and the strongest air traffic between 40° and 53°N. The deviations of the ADS-B message rate in Figure 9b are generally greater than in Figure 8b, as the values are calculated with smaller sample sizes due to the splitting according to geographic latitude. The strongest deviations occur between 42° and 50°N during night time, but smaller deviations are also observed northward of 50°N. The maximum deviation occurs during the storm main phase at 11 May 2024, but the results cannot be interpreted as directly as in Figure 8. For that reason, the ADS-B message rate residuals are calculated based on a simple moving-average model. In addition to removing the dominant diurnal variation, this approach allows to identify increases and decreases in the rate. Figure 9c shows the results, which indicate an increased loss of messages

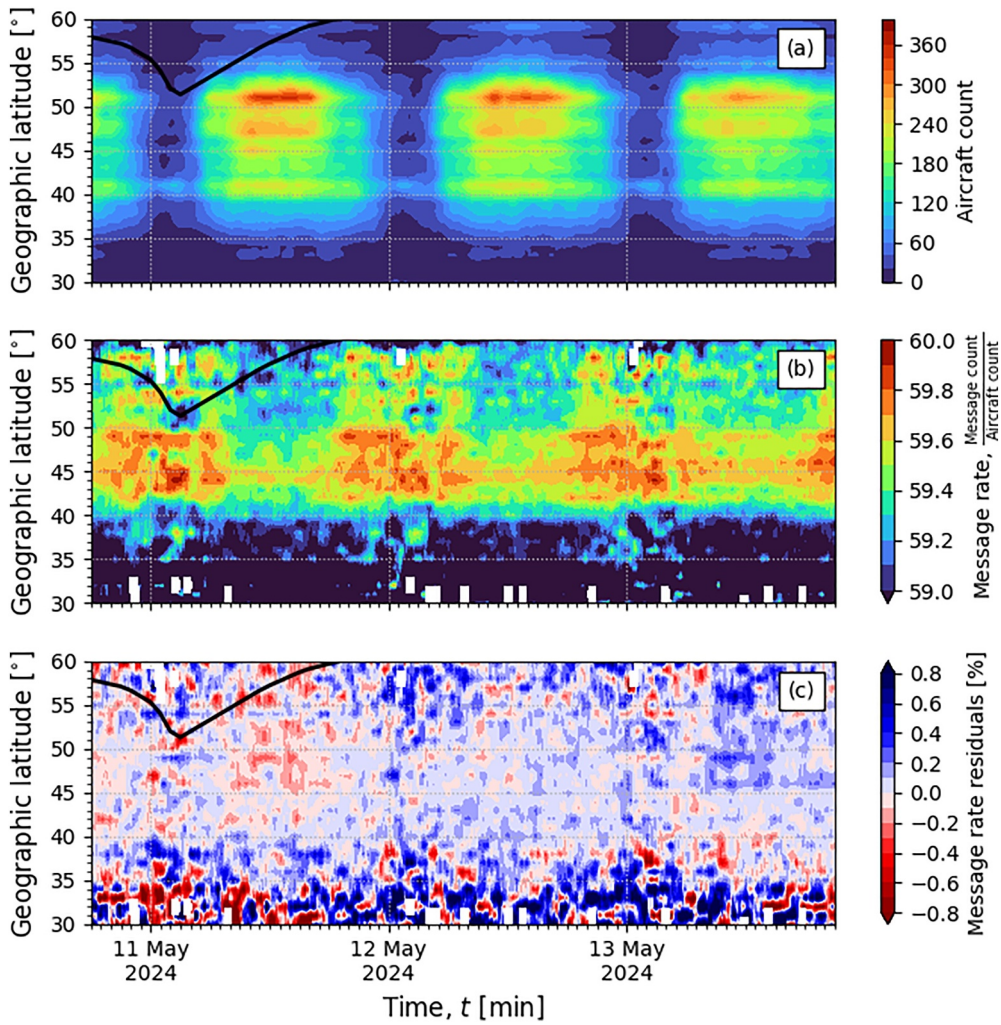

Figure 9. The aircraft count (a), ADS-B message rate (b) and residuals (c) calculated between 10°W and 30°E. The black curve indicates the furthest extent of TEC perturbations from high to mid latitudes as shown in Figure 3.

between 40° and 55°N during 11 May 2024 compared to the other days. The strong residuals northward of 55°N and southward of 40°N are expected due to the lower aircraft counts, nonetheless these regions show a notable loss of messages during 11 May 2024. A significant increase of the loss is also observed along the estimated extent of TEC perturbations (see black curve according Figure 3). However, this may be coincidental and cannot be reliably analyzed, as the aircraft count is too small at these latitudes. A similar and even more pronounced drop in the message rate is observed south of 37°N, but also relates to very small aircraft counts. But this opens up an interesting question for future studies that could investigate such a correlation for regions where storm-driven TEC perturbations and dense air traffic are present.

Similar to the message rate, it would be desirable to have a parameter that describes an average position error for the entire region. This could be implemented by simple trajectory analyses or solved by complex anomaly detection methods (Basora et al., 2019). However, these approaches are not feasible with the large amount of data available and are therefore only useful if a preselection of specific tracks is performed or if the time period is considerably limited (e.g., investigation of a single solar flare). Both steps are applied for the further analysis, which investigates the solar flare during 11 May 2024 from 11:15 to 12:05 UT (see Figure 4). During this period, about 2500 aircraft are tracked across Europe, which allows automatic detection methods for anomalies but also a manual evaluation of the tracks. The result of that evaluation is 190 tracks (7.6%) with identifiable anomalies due to various processes (possibly including space weather impacts).

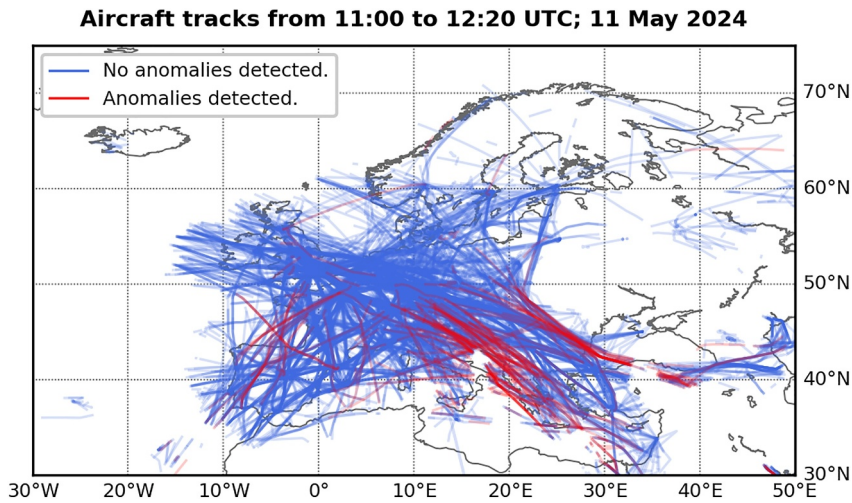

Figure 10. Flight tracks during 11 May 2024 from 11:00 to 12:20 UT without (blue) and with anomalies (red).

Figure 10 shows all tracks without (blue) and with anomalies (red) during the solar flare. A large number of impacted tracks is identified between 40° and 50°N as well as 10° and 40°E with two distinct data gaps in the southern Adriatic Sea and south of the Black Sea. All tracks passing these regions are interrupted, which is likely due to the lack of ADS-B receiver coverage or human-made GNSS signal jamming, commonly observed in this part of Europe. Therefore, similar impacts must be considered for all tracks in regions with less coverage like for example, aircraft passing longer distances over seas. This in turn further decreases the number of suitable tracks for the space weather analysis. Nevertheless, several tracks with anomalies show disturbances only during the solar flare with features described in preceding studies during another event (Schmölter et al., 2025).

Figure 11 shows different examples for tracks with anomalies related to degraded GNSS performance. The causes of these anomalies can be various processes (Pik et al., 2024; Syd Ali et al., 2015; Tabassum et al., 2017) including space weather (Schmölter et al., 2025) with its direct and indirect impacts during the selected solar flare (see Figure 4). The flight track in Figure 11a shows several small lateral deviations (examples marked with arrows) in different directions. The extent of these deviations varies over time and, as in the example shown, is particularly noticeable during the solar flare. The disturbance is therefore not solely driven by the solar flare, but may be amplified by its impact. The second example flight track in Figure 11b shows a combination of data gaps and an offset in reported positions from the predicted track. The length of these data gaps (combined length of approximately 15 min) is extreme considering how rarely such events occur (Tabassum et al., 2017) and that ADS-B receiver coverage in this region (Southern Germany) should be without interruption. Similar examples were investigated by preceding studies during another solar flare, which showed signal interference and ionospheric perturbations causing the combination of data gaps and position errors (Schmölter et al., 2025). The next flight track in Figure 11c also shows an offset from the predicted track during the solar flare peak. This occurs without data gaps, lasts only 11 s, but results in positions with an extreme lateral deviation of approximately 700 km. Large position errors may occur during solar flare due cycle slips or signal loss, which in turn cause deteriorated satellite-receiver geometry and discontinuities of the receiver's lock on the GNSS signals (Muhammad et al., 2015; Zhou et al., 2018). However, this particular anomaly exceeds what is expected for such impacts and an detailed investigation of the GNSS performance would be of interest to understand the interactions causing such extreme deviations. But this would require the raw data from the GNSS receiver on board the aircraft.

The last example in Figure 11d shows the reported positions of an aircraft during ground time. Taking into account the efforts to describe anomalies for in-flight aircraft, it is apparent that aircraft on ground might provide the most straightforward approach to analyze the impact of space weather. Parking aircraft represent stationary receivers and allow the evaluation of the GNSS performance (indicating also the performance for nearby in-flight aircraft). Of course, other effects must be considered (e.g., changing multipath propagation), but their impact could be minimized, for example, by checking the position and movement of nearby aircraft on the ground. Figure 11d shows the error ellipses in addition to the reported positions during (red) and before as well as after

10.1029/2025SW004718

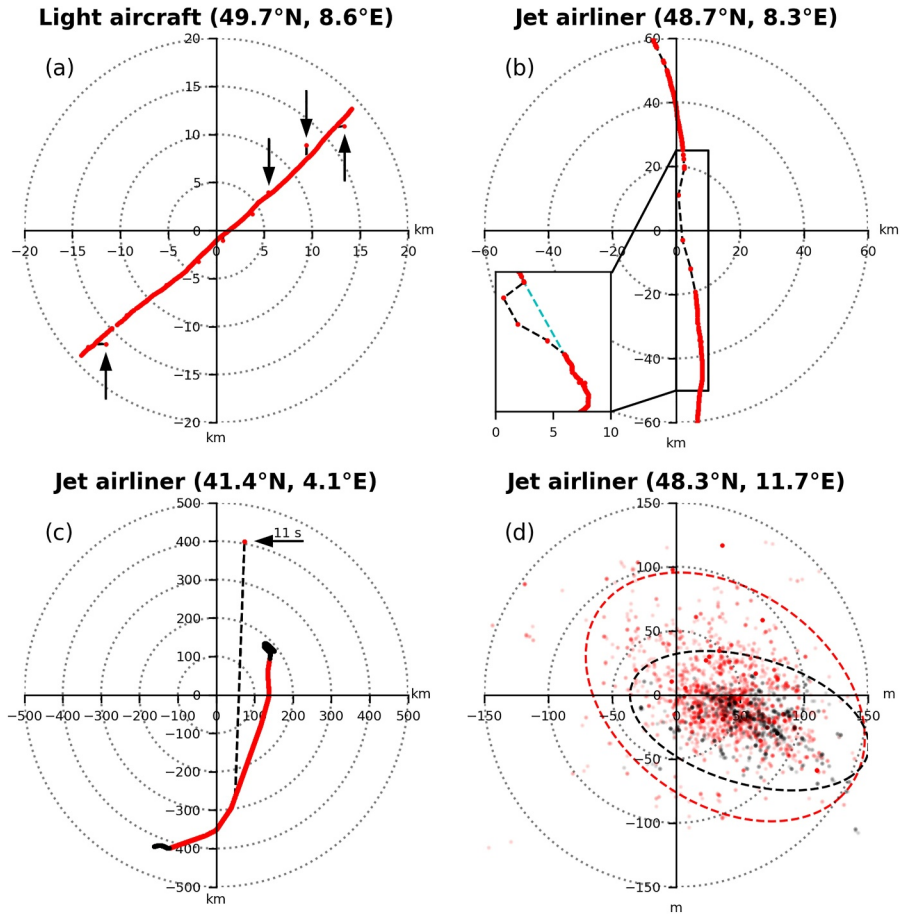

Figure 11. Each panel shows a flight track with reported positions errors during the solar flare 11 May 2024 from 11:15 to 12:05 UT. Panel (a) shows a track with several lateral deviations, panel (b) shows an offset (predicted track in cyan) and significant data gaps along a track, panel (c) shows an extreme position error for 11 s and panel (d) shows the error ellipses of an aircraft during ground time. Reported positions before and after the solar flare are shown with black dots. Red dots are reported positions during the flare. This color coding is also applied for the error ellipses.

(black) the solar flare. The mean position of the aircraft changes negligibly, but the deviation increases noticeably (35.2%). A significantly degraded GNSS performance is therefore observed during the solar flare.

Figure 12 shows two example flight tracks with data gaps. The flight track in Figure 12a shows two gaps, which coincide with the radio flux peaks (see Figure 4a). This could indicate interference for the GNSS or ADS-B signals (Schmölter et al., 2025). The second flight track in Figure 12b shows several gaps of different length, which also coincide around the solar flare peak. Further flight tracks with such data gaps occur during the solar flare.

Hereinafter, the impact of the solar flare on ADS-B in the European region is roughly estimated. For that purpose, two parameters are calculated, which allow insights to the number of data gaps and position errors. The calculation of these parameters requires filtering out those flight tracks that have data gaps before and after the solar flare and those that generally report no reliable positions. This reduces the number of aircraft that are applied to the analysis, but it ensures that only the space weather impact is extracted.

The approach to investigate data gaps calculates the average number of ADS-B messages per minute for all available aircraft. Figure 13a shows the changes of this message rate during the solar flare with a strong decrease the initial phase of the event from 11:22 to 11:30 UT. The minimum value is significantly lower than the mean during the flare (dashed line) and undisturbed (dotted line) periods. In total a loss of approximately 2400 messages occurs from 11:22 to 11:30 UT (equivalent to 40 min without flight tracking accumulated by several aircraft). The impacted flight tracks are shown in Figure 13b from 11:15 to 12:05 UT (black lines) and the last reported positions

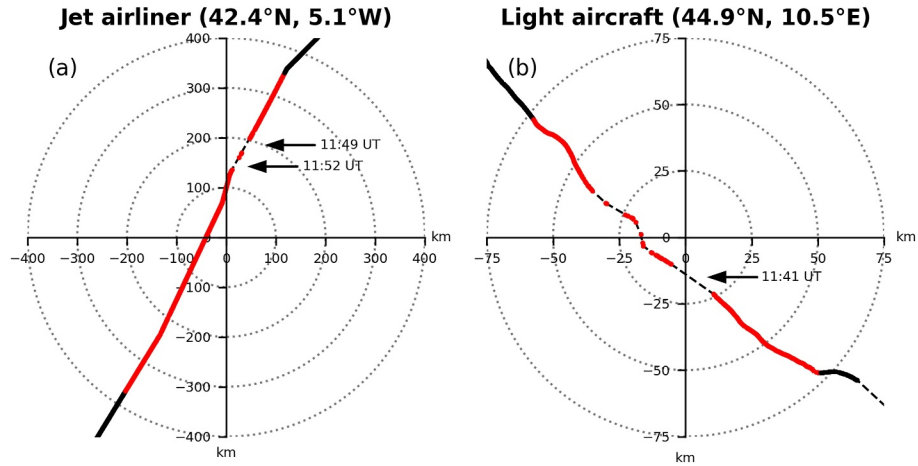

Figure 12. Each panel shows a flight track with reported data gaps during the solar flare 11 May 2024 from 11:15 to 12:05 UT. Panel (a) shows a track with two data gaps and panel (b) shows a track with several data gaps of different length. Reported positions before and after the solar flare are shown with black dots. Red dots are reported positions during the flare.

before data gaps during the solar flare are marked (red dot along each black line). The number is significantly smaller than the manual evaluation of anomalies, which is likely due to the rigorous filtering. However, this is necessary as otherwise the results are too noisy (e.g., due to aircraft passing through regions with poor ADS-B receiver coverage). Furthermore, not every signal loss may be recorded due to the ADS-B raw data sampling rate of 1 Hz. Nevertheless, the parameter in Figure 13a, which should be rather constant according to the applied filters, shows significant variations during the solar flare.

While data gaps are self-explanatory features that can be used for analyses, position errors must first be defined, calculated for all tracks and can only then be used to estimate the number of space weather-driven anomalies throughout the European region. Sophisticated approaches for this are available (Basora et al., 2019), but would require excessive processing time to provide results. Furthermore, these approaches remove some ADS-B data errors that could be relevant for the present study. For this reason, rather simple parameters, that are calculated from the reported positions with short processing time, are applied.

The geodesic distance *ds* between reported positions along tracks can be calculated with different precision depending on the chosen reference system. The analysis of the distance over time *ds*/*dt* ensures that data gaps (increase of *dt* between positions), which might otherwise be mistaken for abrupt position "jumps", are appropriately handled. Position errors driven by degraded GNSS performance, on the other hand, appear as sudden

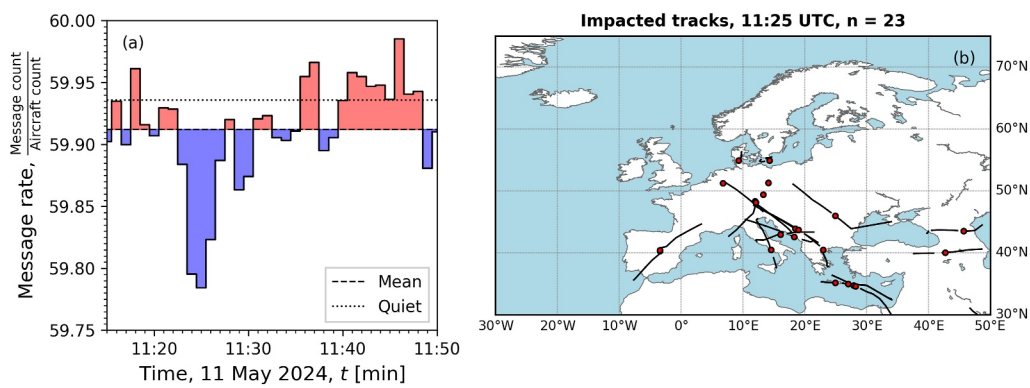

Figure 13. Message rate statistics of the 11 May 2024 solar flare impact on aircraft in the European region from 11:15 to 12:05 UT. Panel (a) shows the message rate averaged for all aircraft with its difference (red and blue shading) from the mean of this rate during the solar flare period. The mean for undisturbed conditions from the previous day is indicated with the dotted line. Panel (b) shows the 23 tracks that only have data gaps during the solar flare. The reported positions during the flare peak are marked with a red dot along the tracks.

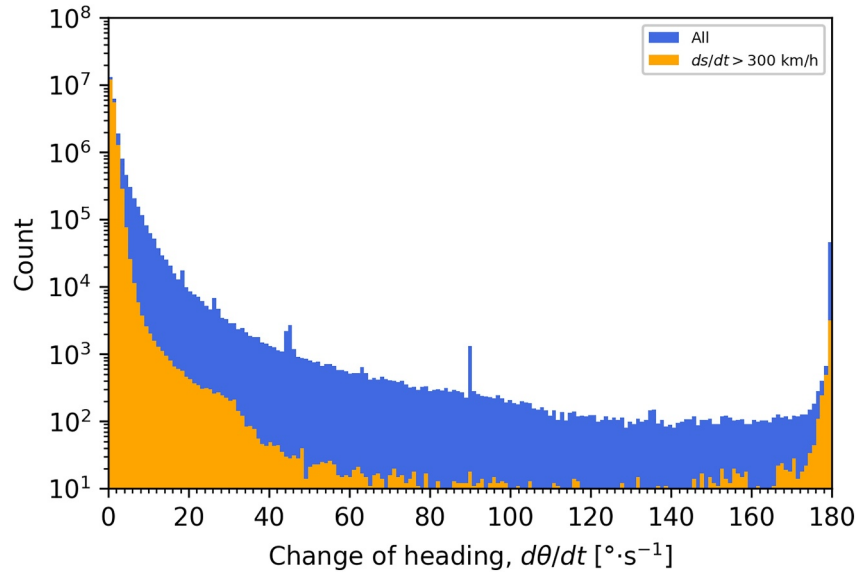

Figure 14. Histogram of the change of the heading $d\theta/dt$ for all data during 11 May 2024 from 11:15 to 12:05 UT (blue) and those corresponding to aircraft with ground speeds greater than 300 km·h^{-1} (orange).

increases due to ds changes, which are appropriately reflected by ds/dt. Some of these increases exceed the feasible acceleration capabilities of aircraft (see Figure 11a), and thus directly identify anomalies. In most cases, however, the variation must be investigated in detail. Further, each ds change is combined with a change in the flight direction $d\theta$, which is calculated along the flight tracks as well. This parameter requires short processing times and is particularly well suited for small changes in ds/dt, as the majority of falsely reported $d\theta$ deviations are subsequently accompanied by an approximate 180° change when the anomaly ends (see Figure 11b). This results in a very simple and effective filter for position errors.

The histogram for $d\theta/dt$ during 11 May 2024 from 11:15 to 12:05 UT in Figure 14 emphasizes the occurrence of anomalous changes in heading during position "jumps". If all aircraft are considered (blue histogram), including those on the ground, then small changes in $d\theta/dt$ dominate and there is an exponential decrease for increasing $d\theta/dt$. Nevertheless, $d\theta/dt$ records occur over the entire range of values. Above approximately 170°·s^{-1}, the number then increases rapidly again, which is due to the anomalies that occur. If the data are filtered for in-flight aircraft (corresponding ds/dt greater than 300 km·h^{-1}), then the distribution changes (yellow histogram). In general, the number is strongly decreased between 3 and 175°·s^{-1}. Thus, small $d\theta/dt$ dominate the distribution even more. The increase at $d\theta/dt$ greater than 170°·s^{-1} is stronger pronounced as well. These results confirm the expectation that in-flight aircraft generally perform only small course changes, and that position errors introduce falsely reported $d\theta$ of approximately 180°.

Similar to the message rate in Figure 13a, a "jump" rate can also be calculated for all available in-flight aircraft (ds/dt greater than 100 km·h^{-1}). The threshold of 170°·s^{-1} is applied to identify the discussed anomalies. This cannot capture all position errors, since $d\theta/dt$ may be smaller for longer offsets (see Figure 11b). However, lower thresholds for $d\theta/dt$ would identify actual flight maneuvers and are therefore not appropriate for the analysis. Figure 15a shows the "jump" rate during the solar flare 11 May 2024 from 11:15 to 12:05 UT. The rate varies strongly and shows a notable increase during the initial phase of the solar flare from 11:18 to 11:27 UT. This corresponds roughly to the time period when most data gaps are observed (see Figure 12a). It should be noted that the mean rate during the solar flare (dashed line) is significantly increased compared to the mean for undisturbed conditions (dotted line). This suggests that the position errors result from both the solar flare (interference) and the overarching geomagnetic storm (ionospheric perturbations). The impacted flight tracks are shown in Figure 15b from 11:15 to 12:05 UT (black lines) and the reported positions during the flare peak are marked (red dot along each black line). The identified "jumps" vary strongly and occur mainly for aircraft between 10°W and 15°E up to the latitude of 55°N. These aircraft are more likely to be impacted by the solar flare due to smaller solar zenith

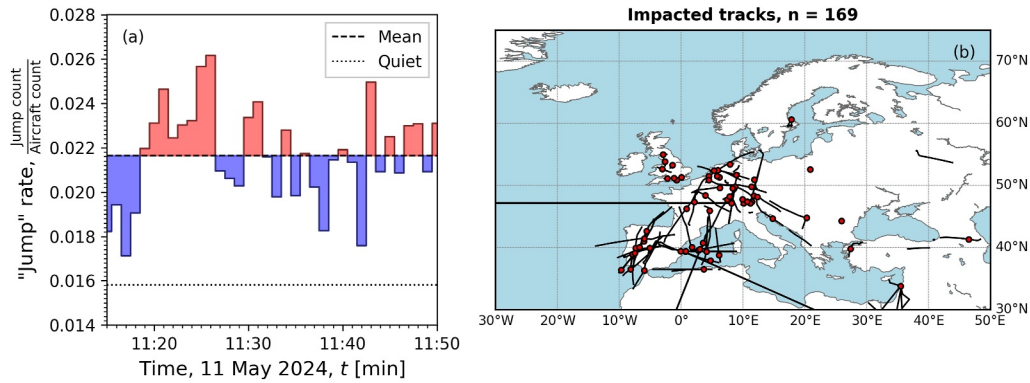

Figure 15. "Jump" rate statistics of the 11 May 2024 solar flare impact on aircraft in the European region from 11:15 to 12:05 UT. Panel (a) shows the "jump" rate averaged for all aircraft with its difference (red and blue shading) from the mean of this rate during the solar flare period. The mean for undisturbed conditions from the previous day is indicated with the dotted line. Panel (b) shows the 169 tracks that have position errors due to "jumps" during the solar flare. The reported positions during the flare peak are marked with a red dot along the tracks.

angles compared to other regions. This is also in good agreement with the impact of the solar flare on the number of IPP in Figure 4c, which shows a strong decrease in the same region.

As shown in Figure 11d, aircraft on the ground provide a particularly simple method of estimating position errors, as they can be analyzed in a similar way to reference stations. For this purpose, the median position is set as the reference, whereby $RMSE_{Pos}$ is calculated according to Equation 1 ($RMSE_{U\text{-}D} = 0$ m). The selection process of suitable aircraft is partially automated (reported positions within a limited radius) but is ensured by an additional manual check for the purpose of this study. The distribution of the selected aircraft reflects the locations of European airports, resulting in a more pronounced spatial clustering (compared to Figure 7c). The resulting lateral $RMSE_{Pos}$ at each aircraft position and an interpolated map are shown in Figure 16.$RMSE_{Pos}$ of different aircraft varies in smaller regions (e.g., area around Munich with several airports), but large-scale variations indicating changes with geographic latitude occur as well. There is a notable increase in $RMSE_{Pos}$ west of 20°E and south of 45°N. North of this latitude, increases are sporadic, such as in the southern United Kingdom of Great Britain. Overall, the results based on ADS-B data show variations broadly consistent with those observed at the reference stations shown in Figure 6. The ionospheric influence on the positioning in aviation is therefore clearly demonstrated. An analysis of the temporal variation of $RMSE_{Pos}$ would be of interest to investigate the impact of the geomagnetic storm, but the number of tracked aircraft is not sufficient at all times and across different latitudes.

4. Discussion

In this study, the defined parameters, message and "jump" rate (see Figures 13 and 15), identified approximately 1.26% of the aircraft with anomalous ADS-B tracks during the solar flare. The manual evaluation identified a larger share of 2.55%. Not all of these anomalies found are driven by space weather, but there is a distinct variation for both, data gaps and position errors, that correlates with the selected solar flare during the Mother's day storm. The impacts of the geomagnetic storm, which lasted several days, are difficult to quantify. However, Figure 8b shows that the decrease in data gaps during this period is much more pronounced than during the solar flare. A similarly strong impact is expected for the positions reported via ADS-B, since the degraded GNSS performance throughout the European region is confirmed via the available reference stations (see Figure 6). Thus, an investigation of anomalies during the entire Mother's day storm would be of interest. For that reason, the challenges of conducting such a detailed analysis over extended periods are discussed in the next paragraphs from both scientific and technical perspectives.

Several characteristics of the ADS-B data set cause challenges for reliable anomaly identification, which results in inclusion of only a subset of anomalies types and a possibly large number of missed but impacted aircraft. The main challenge are the varying geometries of flight tracks, which may share features during flight phases, among aircraft types or in different regions. Furthermore, the ADS-B data are available as a "black-box" data set with no

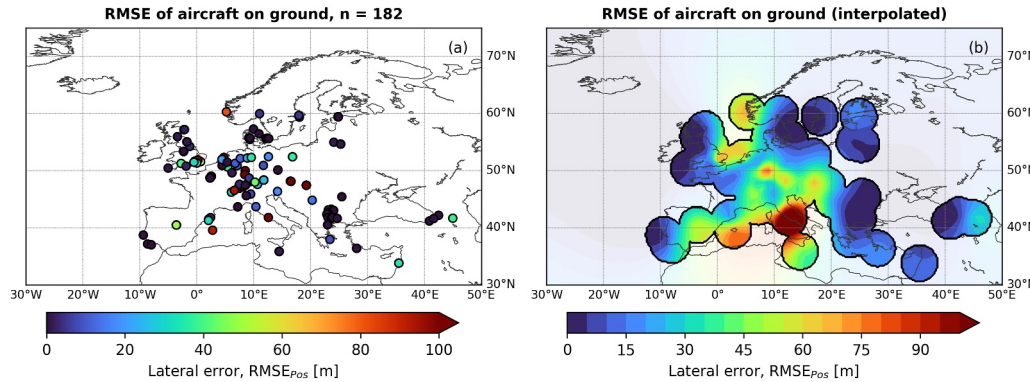

Figure 16. The root mean square errors of the ADS-B reported positions $RMSE_{Pos}$ for the 182 aircraft on ground across Europe during the solar flare 11 May 2024 from 11:15 to 12:05 UT (a). The interpolated map (radial basis function interpolation with linear kernel) highlights spatial variations (b). Regions of the interpolated map, that are further away than 2.5° from the next aircraft and cannot be reliably interpreted, are masked.

information regarding the processing and data generation. Space, air and ground segment cannot be separated, since raw GNSS data from the receivers on board aircraft or data from the individual ADS-B receivers are not available. The specific space weather impacts on ADS-B tracking and the involved segments can therefore only be explained with independent data sets (e.g., data from GNSS reference stations). On the other hand, ADS-B tracking provides a huge amount of data for space weather studies, that are integrated in the work of many users in aviation. This enables highly application-oriented research.

It should be noted that the difficulties of a long-term analysis (several days of the storm) are not mainly caused by a lack of approaches or quality of the data, but rather by the processing time. There can be up to 40 million ADS-B messages per hour and the calculation of flight trajectories or parameters based on them in combination with all the necessary steps requires a lot of processing time. This is beyond the scope of the present or preceding studies and requires analysis on high-performance clusters with parallel processing.

The required basis for such a statistical analysis of longer periods is established via a local database containing ADS-B data from 2023 onward for 9 geomagnetic storms, 41 solar flares and 47 random quiet periods. In addition, various algorithms are available to identify anomalies, including the simple approach presented in this study and, for example, a complex machine-learning method that was successfully applied to Automatic Identification System (AIS) data for maritime traffic (S. K. Singh & Heymann, 2020). The results of the preceding study by Schmölter et al. (2025) with detailed analysis of specific flight tracks and the present study are also crucial for the next steps. Analyzing features along individual flight tracks allows for precise characterization of localized variations, which is crucial to accurately describe and interpret anomalies in the data. This allows further to evaluate the reliability of future statistical analyses over large-scale processes.

The preliminary analyses of ADS data in this and preceding studies indicate that TEC maps cannot sufficiently identify all space weather impacts. Instead derived parameters such as ionospheric gradients are needed to identify perturbations relevant for aircraft surveillance (Schmölter & Berdermann, 2024b). Further, the analysis of solar flare events may require specific indicators, that are optimized to identify impacted regions. Figure 17a shows the by Schmölter and Berdermann (2024a) proposed flare indicator, which considers the absorption based on the solar X-ray flux, solar zenith angle and pre-flare ionospheric state. Thus, while considering only the solar zenith angle would suggest an increase of perturbations toward the center of the dayside, this indicator instead highlights regions where weaker ionization can lead to significant variations. For the solar flare on 11 May 2024, this predicts disturbances in Central Europe that correspond well with the results shown in Figures 15 and 16. The gradients in Figure 17b show increases at approximately 37° and 43°N as well as sporadically north of these geographic latitudes. Interestingly, some stronger gradients are coincidentally in good agreement with increases in the $RMSE_{Pos}$ of aircraft on ground as shown in Figure 16 (e.g., 55°N and 5°E, 59°N and 10°E, as well as 45°N and 15°E). This correlation was shown in detail by Schmölter and Berdermann (2024b) and Schmölter et al. (2025) along selected flight tracks and via statistical analysis. However, further analysis with the available ADS-B data and the proposed methods could result in further insights into spatial variations. Such an

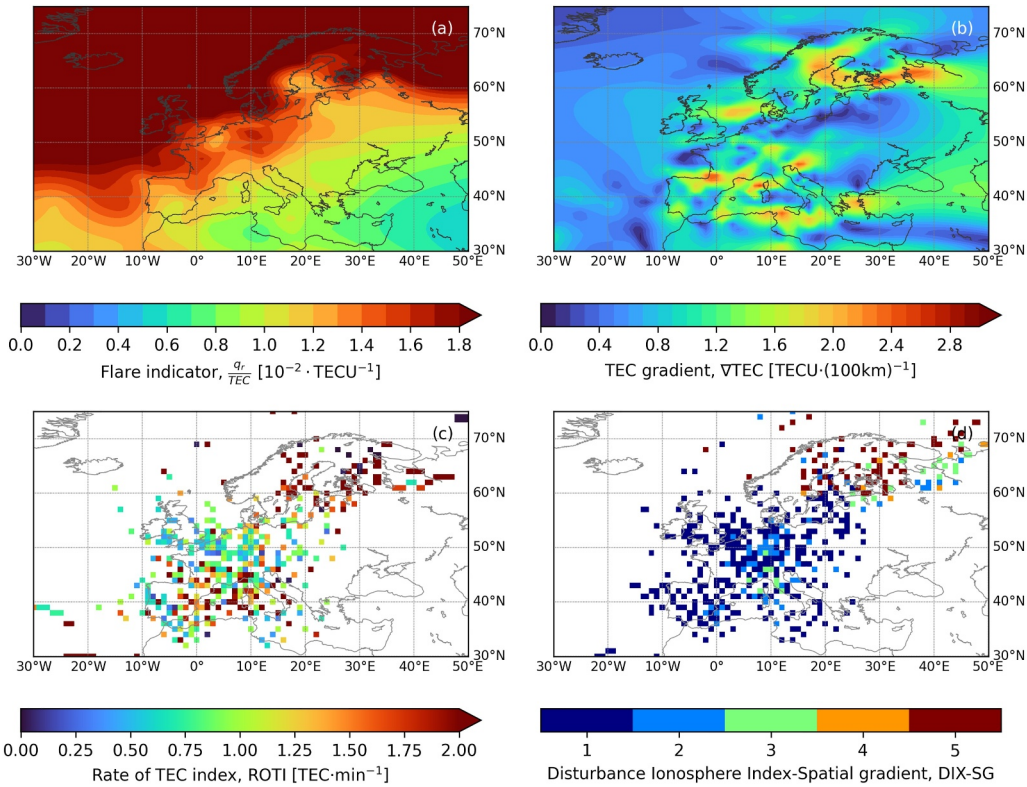

Figure 17. Flare indicator q_r/TEC map (a), which is calculated with the modeled energy absorption q_r during the solar flare and the pre-flare TEC, TEC gradient ∇TEC map (b), rate of TEC index (ROTI) map (c) and disturbance ionosphere index-spatial gradient (DIX-SG) map (d). All maps describe the ionospheric state at the beginning of the solar flare 11 May 2024 at 11:15 UT.

investigation could also identify or improve space weather products that are well-suited to predict space weather impacts in aviation.

Other established ionospheric parameters, including the rate of TEC index (ROTI, see Figure 17c), which can be applied to characterize plasma bubbles (Carmo et al., 2021; Sori et al., 2021), or the disturbance ionosphere index-spatial gradient (DIX-SG, see Figure 17d), which can be applied to characterize further ionospheric variations of small to medium scales (Wilken et al., 2018; Zhao et al., 2025), may also be suitable for more detailed investigations. The interaction between small-scale variations, particularly plasma bubbles, and GNSS-dependent aviation systems can degrade their performance (Saito & Yoshihara, 2017; Tsujii et al., 2014). The findings of this study suggest that ADS-B data are an interesting data set for analysis of potential correlations with such phenomena.

5. Conclusion

During the Mother's Day storm, the ionosphere over the European region experienced various disturbances with temporal and spatial features that are shown in Figures 3 and 6. These findings are in good agreement with preceding studies (Lee et al., 2025; Pal et al., 2025; Paul, Haralambous, et al., 2025; Paul, Moses, et al., 2025) and imply potential impacts for communication and navigation systems that are crucial to aviation operations. Figures 5 and 6 confirm these impacts for GNSS reference stations with degraded performance especially during X-class solar flares and the storm sudden commencement.

An impact on ADS-B tracking is indicated with the averaged message rate (see Figures 8 and 9) decreasing during the 11 May 2024. Further, the analysis of anomalies along flight tracks during a *X*-class solar flare reveals various position errors and data gaps (see Figures 11 and 12), that coincide strongly with the flare peak. The number of these anomalies is estimated over time (see Figures 13 and 15) showing a significant increase for both, data gaps

and position errors, during the solar flare. These results agree well with previous studies on space weather-driven anomalies in ADS systems (Schmölter & Berdermann, 2024b; Schmölter et al., 2025) indicating that 1.26%–2.55% of flight tracks are impacted by the disruptions examined. A higher rate is expected for more advanced anomaly detection algorithms, which should be implemented in future studies.

The analysis of aircraft during ground time allows for a straightforward yet insightful analysis similar to that of the performance of GNSS reference stations (see Figure 16). The results show spatial variations with similar features as observed via TEC derived parameters (see Figure 17). Therefore, this approach offers an interesting opportunity to investigate the GNSS performance via ADS-B and should be utilized in future studies.

Conflict of Interest

The authors declare no conflicts of interest relevant to this study.

Data Availability Statement

OMNI data were obtained from the GSFC/SPDF OMNIWeb interface at https://omniweb.gsfc.nasa.gov/form/dx1.html. GOES-R data were obtained from the NOAA GOES-R Space Weather web interface at https://www.ngdc.noaa.gov/stp/satellite/goes-r.html. ACE MAG and ACE SWEPAM data were obtained from the NASA ASC interface at http://www.srl.caltech.edu/ACE/ASC/level2/index.html. GOW SFX data were obtained from the BKG web interface at https://weltraumwetter.bkg.bund.de. TEC maps were obtained from the IMPC web interface at https://impc.dlr.de. ADS-B tracks were obtained via the OpenSky historical database, which is introduced at https://opensky-network.org/data.

Acknowledgments
We thank NASA for providing easy access to common data in space physics through OMNIWeb. We thank NOAA and the GOES-R program for making the X-ray and EUV satellite data available, the ACE MAG and SWEPAM instrument team as well as the ACE Science Center for providing the solar wind and IMF data, and the BKG GOW for the access to solar radio flux measurements and the successful collaborative research work. We further thank OpenSky Network for the access to historical ADS-B data, which allows application focused space weather research. This work was supported by the Impulsprojekt IN2ACTION (Insight, Information, Action) of the German Aerospace Center (DLR). Open Access funding enabled and organized by Projekt DEAL.

References

Ang, D. J., Buhari, S. M., Abdullah, M., & Bahari, S. A. (2025). The effects of solar flares and geomagnetic storm on the upper and lower ionosphere across the Malay archipelago between 8th and 15th May 2024. *Journal of Geophysical Research: Space Physics*, *130*(4), e2024JA033601. https://doi.org/10.1029/2024ja033601

ASC. (2025). ACE level 2 (verified) data [Dataset]. Retrieved from https://izw1.caltech.edu/ACE/ASC/level2/index.html

Basora, L., Olive, X., & Dubot, T. (2019). Recent advances in anomaly detection methods applied to aviation. *Aerospace*, *6*(11), 117. https://doi.org/10.3390/aerospace6110117

Berdermann, J., Kriegel, M., Banyś, D., Heymann, F., Hoque, M. M., Wilken, V., et al. (2018). Ionospheric response to the X9.3 flare on 6 September 2017 and its implication for navigation services over Europe. *Space Weather*, *16*(10), 1604–1615. https://doi.org/10.1029/2018sw001933

Bezerra, L. d. S., de Oliveira, P. S., & Krueger, C. P. (2025). Performance analysis of multi-GNSS PPP under the effects of extreme geomagnetic event: A case study of Mother's day solar storm (10–15 May 2024). *Advances in Space Research*, *76*(12), 1–17. https://doi.org/10.1016/j.asr.2025.06.036

Binder, F., Bauer, D. J., Pany, T., & Schüler, T. (2025). Performance analysis of CUDA-based Galileo signal quality monitoring. In *European navigation conference 2024*. MDPI. https://doi.org/10.3390/engproc2025088054.54

BKG. (2025). Space weather observation at the geodetic observatory Wettzell [Dataset]. Retrieved from https://weltraumwetter.bkg.bund.de/

Cane, H. V., & Richardson, I. G. (2003). Interplanetary coronal mass ejections in the near-Earth solar wind during 1996–2002. *Journal of Geophysical Research*, *108*(A4), 1156. https://doi.org/10.1029/2002ja009817

Carmo, C. S., Denardini, C. M., Figueiredo, C. A. O. B., Resende, L. C. A., Picanço, G. A. S., Barbosa Neto, P. F., et al. (2021). Evaluation of different methods for calculating the ROTI index over the Brazilian sector. *Radio Science*, *56*(8), e2020RS007140. https://doi.org/10.1029/2020rs007140

Chamberlin, P. C., Woods, T. N., Eparvier, F. G., & Jones, A. R. (2009). Next generation x-ray sensor (XRS) for the NOAA GOES-R satellite series. In S. Fineschi & J. A. Fennelly (Eds.), *SPIE proceedings. SPIE*. https://doi.org/10.1117/12.826807

Chen, Z., Gao, Y., & Liu, Z. (2005). Evaluation of solar radio bursts' effect on GPS receiver signal tracking within international GPS service network. *Radio Science*, *40*(3), 1–11. https://doi.org/10.1029/2004rs003066

Danilchuk, E., Yasyukevich, Y., Vesnin, A., Klyusilov, A., & Zhang, B. (2025). Impact of the May 2024 extreme geomagnetic storm on the ionosphere and GNSS positioning. *Remote Sensing*, *17*(9), 1492. https://doi.org/10.3390/rs17091492

De Michelis, P., & Consolini, G. (2025). Unveiling the Gannon storm: How ground-based magnetometers mapped its global impact. *Space Weather*, *23*(6), e2025SW004350. https://doi.org/10.1029/2025sw004350

Eparvier, F. G., Crotser, D., Jones, A. R., McClintock, W. E., Snow, M., & Woods, T. N. (2009). The extreme ultraviolet sensor (EUVS) for GOES-R. In S. Fineschi & J. A. Fennelly (Eds.), *SPIE proceedings. SPIE*. https://doi.org/10.1117/12.826445

Garrard, T. L., Davis, A. J., Hammond, J. S., & Sears, S. R. (1998). The ACE science center. *Space Science Reviews*, *86*(1/4), 649–663. https://doi.org/10.1023/a:1005096317576

GFZ. (2025). German research centre for geosciences–Geomagnetic *Kp* index [Dataset]. Retrieved from https://kp.gfz-potsdam.de/

Gonzalez-Esparza, J. A., Sanchez-Garcia, E., Sergeeva, M., Corona-Romero, P., Gonzalez-Mendez, L. X., Valdes-Galicia, J. F., et al. (2024). The mother's day geomagnetic storm on 10 May 2024: Aurora observations and low latitude space weather effects in Mexico. *Space Weather*, *22*(11), e2024SW004111. https://doi.org/10.1029/2024sw004111

ICAO. (2014). ADS-B implementation and operations guidance document [Computer software manual]. In *Robert-Bourassa boulevard*, 7th ed. Montréal. Retrieved from https://www.icao.int/APAC/Documents/edocs/cns/ADSB_AIGD7.pdf

ICAO. (2016). Global operational data link (GOLD) manual [Computer software manual]. In *Robert-bourassa boulevard*, 1st ed. Montréal. Retrieved from https://www.skybrary.aero/sites/default/files/bookshelf/4134.pdf

IMPC. (2025). Ionosphere monitoring and prediction center–Products [Dataset]. Retrieved from https://impc.dlr.de/products
Ishii, M., Berdermann, J., Forte, B., Hapgood, M., Bisi, M. M., & Romano, V. (2024). Space weather impact on radio communication and navigation. *Advances in Space Research*. https://doi.org/10.1016/j.asr.2024.01.043
Jakowski, N., & Jungstand, A. (1994). Modelling the regional ionosphere by using GPS observations. In *Paper presented at international beacon satellite symposium*. Retrieved from https://elib.dlr.de/23684/
Jakowski, N., Mayer, C., Hoque, M. M., & Wilken, V. (2011). Total electron content models and their use in ionosphere monitoring. *Radio Science*, *46*(6). https://doi.org/10.1029/2010rs004620
Kriegel, M., & Berdermann, J. (2020). Ionosphere monitoring and prediction center. In *2020 European navigation conference (Enc)*. IEEE. https://doi.org/10.23919/enc48637.2020.9317443
Kruparova, O., Krupar, V., Szabo, A., Lario, D., Nieves-Chinchilla, T., & Martinez Oliveros, J. C. (2024). Unveiling the interplanetary solar radio bursts of the 2024 mother's day solar storm. *The Astrophysical Journal Letters*, *970*(1), L13. https://doi.org/10.3847/2041-8213/ad5da6
Lee, W., Liu, G., Wu, D. L., & Rowland, D. E. (2025). Ionospheric response to the 10 May 2024 geomagnetic storm as observed in GNSS radio occultation electron density. *Journal of Geophysical Research: Space Physics*, *130*(3), e2024JA033489. https://doi.org/10.1029/2024ja033489
Loewe, C. A., & Prölss, G. W. (1997). Classification and mean behavior of magnetic storms. *Journal of Geophysical Research*, *102*(A7), 14209–14213. https://doi.org/10.1029/96ja04020
Machol, J. L., Eparvier, F. G., Viereck, R. A., Woodraska, D. L., Snow, M., Thiemann, E., et al. (2020). GOES-R series solar X-ray and ultraviolet irradiance. In *The GOES-r series* (pp. 233–242). Elsevier. https://doi.org/10.1016/b978-0-12-814327-8.00019-6
Matzka, J., Bronkalla, O., Tornow, K., Elger, K., & Stolle, C. (2021). Geomagnetic *Kp* index. *GFZ Data Services*. https://doi.org/10.5880/KP.0001
McCallie, D., Butts, J., & Mills, R. (2011). Security analysis of the ADS-B implementation in the next generation air transportation system. *International Journal of Critical Infrastructure Protection*, *4*(2), 78–87. https://doi.org/10.1016/j.ijcip.2011.06.001
McComas, D. J., Bame, S. J., Barker, P., Feldman, W. C., Phillips, J. L., Riley, P., & Griffee, J. W. (1998). Solar wind electron proton alpha monitor (SWEPAM) for the advanced composition explorer. *Space Science Reviews*, *86*(1/4), 563–612. https://doi.org/10.1023/a:1005040232597
Muhammad, B., Alberti, V., Marassi, A., Cianca, E., & Messerotti, M. (2015). Performance assessment of GPS receivers during the September 24, 2011 solar radio burst event. *Journal of Space Weather and Space Climate*, *5*, A32. https://doi.org/10.1051/swsc/2015034
NASA. (2025). National aeronautics and space administration Goddard space Flight center - OMNI data set [Dataset]. *NASA*. Retrieved from https://omniweb.gsfc.nasa.gov/form/dx1.html
NGDC. (2025). GOES-R space weather [Dataset]. *NGDC*. Retrieved from https://www.ngdc.noaa.gov/stp/satellite/goes-r.html
OpenSky. (2025). OpenSky–Historical data [Dataset]. *OpenSky*. Retrieved from https://opensky-network.org/data/trino
Pal, S. K., Sarkar, S., Nanda, K., Sanyal, A., Brawar, B., Datta, A., et al. (2025). Global response of vertical total electron content to mother's day G5 geomagnetic storm of May 2024: Insights from IGS and GIM observations. *Atmosphere*, *16*(5), 529. https://doi.org/10.3390/atmos16050529
Park, J., Spogli, L., Azeez, A., Alfonsi, L., Cesaroni, C., Romano, V., & Akande, A. (2025). The impact of Mother's day storms in May 2024 on precise point positioning at mid-latitudes. *Annals of Geophysics*, *68*(2), A214. https://doi.org/10.4401/ag-9161
Paul, K. S., Haralambous, H., Moses, M., Oikonomou, C., Potirakis, S. M., Bergeot, N., & Chevalier, J.-M. (2025a). Investigation of the ionospheric response on mother's day 2024 geomagnetic superstorm over the European sector. *Atmosphere*, *16*(2), 180. https://doi.org/10.3390/atmos16020180
Paul, K. S., Moses, M., Haralambous, H., & Oikonomou, C. (2025b). Effects of the mother's day superstorm (10–11 May 2024) over the global ionosphere. *Remote Sensing*, *17*(5), 859. https://doi.org/10.3390/rs17050859
Pik, E., Berra, M., Yearwood, J., & Garcia, J. (2024). Detecting GPS anomalies in aviation using ADS-B: Correlating coordinate gaps and GPS deviations with NOTAM warnings. In *Aiaa aviation forum and ascend 2024*. https://doi.org/10.2514/6.2024-4640
Pleninger, S., Hospodka, J., Steiner, J., Lukeš, P., Topková, T., Pilmannová, T., & Kraus, J. (2025). Aircraft resilience to GNSS jamming and impact on ADS-B quality indicators. *Aeronautical Journal*, *129*(1336), 1629–1646. https://doi.org/10.1017/aer.2024.165
Riahi Manesh, M., & Kaabouch, N. (2017). Analysis of vulnerabilities, attacks, countermeasures and overall risk of the automatic dependent surveillance-broadcast (ADS-B) system. *International Journal of Critical Infrastructure Protection*, *19*, 16–31. https://doi.org/10.1016/j.ijcip.2017.10.002
Richardson, I., & Cane, H. (2024). Near-earth interplanetary coronal mass ejections since January 1996. *Online. Harvard Dataverse*. https://doi.org/10.7910/DVN/C2MHTH
Richardson, I. G., & Cane, H. V. (2010). Near-earth interplanetary coronal mass ejections during solar cycle 23 (1996–2009): Catalog and summary of properties. *Solar Physics*, *264*(1), 189–237. https://doi.org/10.1007/s11207-010-9568-6
Saito, S., & Yoshihara, T. (2017). Evaluation of extreme ionospheric total electron content gradient associated with plasma bubbles for GNSS ground-based augmentation system. *Radio Science*, *52*(8), 951–962. https://doi.org/10.1002/2017rs006291
Schäfer, M., Strohmeier, M., Lenders, V., Martinovic, I., & Wilhelm, M. (2014). Bringing up OpenSky: A large-scale ADS-B sensor network for research. In *Ipsn-14 proceedings of the 13th international symposium on information processing in sensor networks* (pp. 83–94). IEEE. https://doi.org/10.1109/ipsn.2014.6846743
Schäfer, M., Strohmeier, M., Leonardi, M., & Lenders, V. (2021). LocaRDS: A localization reference data set. *Sensors*, *21*(16), 5516. https://doi.org/10.3390/s21165516
Schmölter, E., & Berdermann, J. (2024a). Post-event analysis of the 9 February2024 X-Flare. *URSI Radio Science Letters*, *6*, 1–5. https://doi.org/10.46620/24-0016
Schmölter, E., & Berdermann, J. (2024b). Weather and space weather driven variability of ADS-C reports in New Zealand airspace. *IEEE Transactions on Aerospace and Electronic Systems*, 1–22. https://doi.org/10.1109/taes.2024.3423029
Schmölter, E., Berdermann, J., Wilken, V., & Wenzel, D. (2025). Should we monitor space weather effects on surveillance technologies used in air traffic Management? first results. *Space Weather*, *23*(4), e2025SW004352. https://doi.org/10.1029/2025sw004352
Singh, R., Scipión, D. E., Kuyeng, K., Condor, P., De La Jara, C., Velasquez, J. P., et al. (2024). Ionospheric disturbances observed over the Peruvian sector during the mother's day storm (G5-Level) on 10–12 May 2024. *Journal of Geophysical Research: Space Physics*, *129*(11), e2024JA033003. https://doi.org/10.1029/2024ja033003
Singh, S. K., & Heymann, F. (2020). Machine learning-assisted anomaly detection in maritime navigation using AIS data. In *2020 ieee/ion position, location and navigation symposium (plans)* (pp. 832–838). IEEE. https://doi.org/10.1109/plans46316.2020.9109806
Sori, T., Shinbori, A., Otsuka, Y., Tsugawa, T., & Nishioka, M. (2021). The occurrence feature of plasma bubbles in the equatorial to midlatitude ionosphere during geomagnetic storms using long-term GNSS-TEC data. *Journal of Geophysical Research: Space Physics*, *126*(5), e2020JA029010. https://doi.org/10.1029/2020ja029010

Stone, E. C., Frandsen, A. M., Mewaldt, R. A., Christian, E. R., Margolies, D., Ormes, J. F., & Snow, F. (1998). The advanced composition explorer. *Space Science Reviews*, *86*(1/4), 1–22. https://doi.org/10.1023/a:1005082526237

Suraina, Rakhman, A., Abadi, P., Kilowasid, L. O. M. M., Putra, A. Y., Perwitasari, S., & Irnaka, T. M. (2025). Pre-Sunrise equatorial plasma bubble over Indonesia during the 11 May 2024 super geomagnetic storm. *Earth and Space Science*, *12*(6), e2024EA004152. https://doi.org/10.1029/2024ea004152

Syd Ali, B., Schuster, W., Ochieng, W., & Majumdar, A. (2015). Analysis of anomalies in ADS-B and its GPS data. *GPS Solutions*, *20*(3), 429–438. https://doi.org/10.1007/s10291-015-0453-5

Tabassum, A., Allen, N., & Semke, W. (2017). ADS-B message contents evaluation and breakdown of anomalies. In *2017 ieee/aiaa 36th digital avionics systems conference (DASC)* (pp. 1–8). IEEE. https://doi.org/10.1109/dasc.2017.8102001

Tapping, K. F. (2013). The 10.7cm solar radio flux (F10.7). *Space Weather*, *11*(7), 394–406. https://doi.org/10.1002/swe.20064

Tsujii, T., Fujiwara, T., Kubota, T., & Kubo, Y. (2014). Flight test evaluation of INS-Aided GPS tracking performance under strong ionospheric scintillation. *Proceedings of the ISCIE International Symposium on Stochastic Systems Theory and its Applications*, *2014*, 164–170. https://doi.org/10.5687/sss.2014.164

Wang, X., Aa, E., Chen, Y., Zhang, J., Zhu, Y., Cai, L., et al. (2025). Midlatitude neutral wind response during the mother's day super-intense geomagnetic storm in 2024 using observations from the Chinese Meridian Project. *Journal of Geophysical Research: Space Physics*, *130*(4), e2024JA033574. https://doi.org/10.1029/2024ja033574

Wilken, V., Kriegel, M., Jakowski, N., & Berdermann, J. (2018). An ionospheric index suitable for estimating the degree of ionospheric perturbations. *Journal of Space Weather and Space Climate*, *8*, A19. https://doi.org/10.1051/swsc/2018008

Xue, D. (2025). Space weather disrupts aviation. *npj Space Exploration*, *1*(1), 1–3. https://doi.org/10.1038/s44453-025-00011-y

Xue, D., Wu, L., Xu, T., Wu, C., Wang, Z., & He, Z. (2024). Space weather effects on transportation systems: A review of current understanding and future outlook. *Space Weather*, *22*(12), e2024SW004055. https://doi.org/10.1029/2024sw004055

Xue, D., Yang, J., Liu, Z., & Yu, S. (2023). -Examining the economic costs of the 2003 halloween storm effects on the north hemisphere aviation using flight data in 2019. *Space Weather*, *21*(3), e2022SW003381. https://doi.org/10.1029/2022sw003381

Yasyukevich, Y., Astafyeva, E., Padokhin, A., Ivanova, V., Syrovatskii, S., & Podlesnyi, A. (2018). The 6 September 2017 X-Class solar flares and their impacts on the ionosphere, GNSS, and HF radio wave propagation. *Space Weather*, *16*(8), 1013–1027. https://doi.org/10.1029/2018sw001932

Younas, W., Nishimura, Y., Liao, W., Semeter, J. L., Mrak, S., Morton, Y. J., & Groves, K. M. (2025). Spatio-temporal evolution of mid-latitude GPS scintillation and position errors during the May 2024 solar storm. *Journal of Geophysical Research: Space Physics*, *130*(6), e2025JA033839. https://doi.org/10.1029/2025ja033839

Zhao, D., Zhang, X., Zhang, P., Liu, H., Zhang, K., Li, W., et al. (2025). The performance of DIXSG on characterizing global and regional ionospheric disturbances utilizing geodetic receiver Network-A case Study. *Space Weather*, *23*(10), e2024SW004209. https://doi.org/10.1029/2024sw004209

Zhou, W., Gu, S., Ge, M., & Wang, J. (2018). Analysis of the effect of the 06-09-2017 solar flare on GNSS signal and positioning performance. In *China satellite navigation conference (Csnc) 2018 proceedings* (pp. 555–569). Springer. https://doi.org/10.1007/978-981-13-0014-1_46

Zwickl, R. D., Doggett, K. A., Sahm, S., Barrett, W. P., Grubb, R. N., Detman, T. R., et al. (1998). The NOAA real-time solar-wind (RTSW) system using ACE data. *Space Science Reviews*, *86*(1/4), 633–648. https://doi.org/10.1023/a:1005044300738